REPUBLIC OF TÜRKİYE
MUĞLA SITKI KOÇMAN UNIVERSITY
GRADUATE SCHOOL OF NATURAL AND APPLIED SCIENCE

DEPARTMENT OF ELECTRICAL AND ELECTRONICS ENGINEERING

A NOVEL DUAL-BJT AVALANCHE PULSE GENERATOR WITH MIXER EFFECT

MASTER OF SCIENCE (M.Sc.)

EMRAH TELLİ

JANUARY 2023
MUĞLA

REPUBLIC OF TÜRKİYE
MUĞLA SITKI KOÇMAN UNIVERSITY
GRADUATE SCHOOL OF NATURAL AND APPLIED SCIENCE

DEPARTMENT OF ELECTRICAL AND ELECTRONICS ENGINEERING

A NOVEL DUAL-BJT AVALANCHE PULSE GENERATOR WITH MIXER EFFECT

MASTER OF SCIENCE (M.Sc.)

EMRAH TELLİ

JANUARY 2023
MUĞLA

MUĞLA SITKI KOÇMAN UNIVERSITY

Graduate School of Natural and Applied Science

APPROVAL OF THE THESIS

The thesis entitled "**A NOVEL DUAL-BJT AVALANCHE PULSE GENERATOR WITH MIXER EFFECT**" submitted by **EMRAH TELLİ** has been unanimously accepted by the jury members of the 9th of January 2023 to fulfill the requirements for the degree of Master of Science in Electrical and Electronics Engineering Department.

EXAMINING COMMITTEE MEMBERS

Prof. Dr. Bahadır Süleyman YILDIRIM **(Head of Committee, Supervisor)**
Electrical and Electronics Engineering Department,
Muğla Sıtkı Koçman University, Muğla _____

Asst. Prof. Dr. Kutlu KARAYAHŞİ **(Member)**
Electrical and Electronics Engineering Department,
Muğla Sıtkı Koçman University, Muğla _____

Prof. Dr. Emine Yeşim ZORAL **(Member)**
Electrical and Electronics Engineering Department,
Dokuz Eylül University, İzmir _____

APPROVAL OF HEAD OF THE DEPARTMENT

Prof. Dr. Bahadır Süleyman YILDIRIM
Head, Electrical and Electronics Engineering Department,
Muğla Sıtkı Koçman University, Muğla _____

Prof. Dr. Bahadır Süleyman YILDIRIM
Supervisor, Electrical and Electronics Engineering Department,
Muğla Sıtkı Koçman University, Muğla _____

Date: 09/01/2023

I hereby declare that this thesis complies with academic and scientific ethical standards. All of the results, documents, information that I have acquired and presented during my thesis studies have been acquired by me personally and within the purview of this thesis. I further declare that, in accordance with academic and scientific ethical guidelines, all original data and findings that were not discovered during the research for this thesis have been properly referenced.

Emrah TELLİ

09/01/2023

ABSTRACT

A NOVEL DUAL-BJT AVALANCHE PULSE GENERATOR WITH MIXER EFFECT

Emrah TELLİ

Master of Science (M.Sc.)

Graduate School of Natural and Applied Sciences

Dept. of Electrical and Electronics Engineering

Supervisor: Prof. Dr. Bahadır Süleyman YILDIRIM

January 2023, 55 pages

Communications, radar, imaging, and medical-related systems have been demanding innovations in short-pulse creation for many years. The requisition on pulse creation having a short pulse width, high bandwidth, and high pulse amplitude is the main motivation of this thesis. As the answer to these requests, a novel, simple, and efficient pulse generation technique using two BJTs using the avalanche effect is presented in this thesis. The presented design is an improved version of the basic single-transistor avalanche pulse generator, and it composes of two identical pulse generators which drive a common 50 Ω load resistor at the output. The pulse generator circuit utilizes the mixer effect which is inherent to the transistors to broaden the spectrum of the output pulse. Thus, the output signal exhibits wider bandwidth and narrower pulse width, compared to the basic single-transistor circuit. The presented pulse generator also provides increased power output without using any power amplifier. Differently from many referred studies, the generated pulse is a positive short pulse having a Gaussian shape. Another method, using a Schottky diode as a mixer, to create wideband and short pulse signals has also been presented along with the effect of the dc supply voltage V_{CC}. As the next step in research, the basic avalanche pulse generator circuit was modified to control the pulse width and pulse amplitude of the output pulse by injecting a signal having different frequencies to the base of the transistor and by varying the value of the effective avalanche capacitance by incorporating a varactor diode suitably. The results presented in this thesis show that short pulses can be created by achieving a wideband spectrum due to the mixing effect, and the output pulse amplitude and pulse width can be controlled as depicted in the thesis. The experimented circuit topologies can be used in ground-penetrating radar and ultra-wideband communication systems.

Keywords: Short pulse generators, Avalanche transistors, Schottky diodes, Diode mixe

ÖZET

KARIŞTIRICI ETKİSİ İLE YENİ BİR ÇIĞ ETKİLİ ÇİFT BJT DARBE ÜRETECİ

Emrah TELLİ

Yüksek Lisans Tezi

Fen Bilimleri Enstitüsü

Elektrik Elektronik Mühendisliği Ana Bilim Dalı

Danışman: Prof. Dr. Bahadır Süleyman YILDIRIM

Ocak 2023, 55 sayfa

İletişim, radar, görüntüleme ve tıpla ilgili sistemler, uzun yıllardır kısa darbe oluşturmada yenilikler talep etmektedir. Kısa darbe genişliğine, yüksek bant genişliğine ve yüksek darbe genliğine sahip darbe oluşturma gerekliliği bu tezin ana motivasyonudur. Bu isteklere yanıt olarak, bu tezde çığ etkisi ile birlikte iki BJT kullanan yeni, basit ve verimli bir darbe üretim tekniği sunulmaktadır. Sunulan tasarım, temel tek transistörlü çığ darbe üretecinin geliştirilmiş bir versiyonudur ve çıkışta ortak bir 50 Ω yük direncini süren iki özdeş darbe üretecinden oluşur. Darbe üreteci devresi, çıkış darbesinin spektrumunu genişletmek için transistörlerde bulunan karıştırıcı etkisini kullanır. Böylece çıkış sinyali, temel tek transistör devresine kıyasla daha geniş bant genişliği ve daha dar darbe genişliği sergiler. Sunulan darbe üreteci ayrıca herhangi bir güç amplifikatörü kullanmadan artırılmış güç çıkışı sağlar. Bahsedilen birçok çalışmadan farklı olarak, üretilen darbe, Gauss şekline sahip pozitif bir kısa darbedir. Geniş bant ve kısa darbe sinyalleri oluşturmak için karıştırıcı olarak bir Schottky diyot kullanan başka bir yöntem de DC besleme gerilimi V_{CC}'nin etkisi ile birlikte sunulmuştur. Araştırmanın bir sonraki adımı olarak, temel çığ darbe üreteci devresi, transistörün base terminaline farklı frekanslara sahip bir sinyal enjekte ederek ve uygun bir varaktör diyotu dahil ederek efektif çığ kapasitansının değerini değiştirerek çıkış darbesinin darbe genişliğini ve darbe genliğini kontrol edecek şekilde değiştirildi. Bu tezde sunulan sonuçlar, karıştırma etkisi nedeniyle geniş bant spektrumu elde edilerek kısa darbelerin oluşturulabileceğini ve tezde gösterildiği gibi çıkış darbe genliği ve darbe genişliğinin kontrol edilebileceğini göstermektedir. Denenen devre topolojileri, zemine nüfuz eden radar ve ultra geniş bant iletişim sistemlerinde kullanılabilir.

Anahtar Kelimeler: Kısa darbe üreteçleri, Çığ transistörleri, Schottky diyotları, Diyot karıştırıcı

Dedicated to My Family

ACKNOWLEDGEMENT

Sincerely, I would like to start with my supervisor and mentor Prof. Dr. Bahadır S. YILDIRIM, his guidance, encouragement, good willingness, and belief in me were precious, and working with him turned hardness into joy. He is the one who has excellent knowledge and expertise in this particular field, and I am trying to find my way in this light.

I owe a great debt to Prof. Dr. Korkut YEĞİN and Res. Asst. Mustafa PEHLİVAN from Ege University for using the RF Lab, and for their interest and time.

I would like to add my special thanks to examining committee member Asst. Prof. Dr. Kutlu KARAYAHŞİ for his support, patience, and helpful comments. His contributions are well appreciated.

I am also thankful to examining committee member Prof. Dr. Emine Yeşim ZORAL to accept to attend my thesis defense, her considerations of this work, and her valuable comments.

I would like to thank also the other examining committee members Assoc. Prof. Dr. Akın TAŞÇIKARAOĞLU and Asst. Prof. Dr. Mümtaz YILMAZ for their acceptance to be a jury member and their time.

I would like to thank all Professors in Dept. of Electrical and Electronics Engineering at Muğla Sıtkı Koçman University for their understanding and support from the beginning to this very day.

And I am also thankful to my colleagues and friends; Muhammed Ali BEYAZIT and Ali Can ERÜST from Dept. of Electrical and Electronics Engineering. In all stages of my work and also in daily life, I felt their closeness, support, and standing on behalf of me, I am deeply honored to work with these people.

Also, I would like to state that an article named “A NOVEL DUAL-BJT AVALANCHE PULSE GENERATOR WITH MIXER EFFECT” based on a part of this thesis has found worth being published by Cambridge University Press - International Journal of Microwave and Wireless Technologies, the publishment process goes on now. Furthermore, again based on this thesis, a presentation was done at the XIV. Research Symposium coordinated by MSKU Graduate School of Natural and Applied Sciences.

Finally, I owe to present gratitude to my closest friend Refikcan BOZKURT, nothing is more valuable than a true friend standing beside you for life.

Last but not the least, my deepest gratitude has to go to my precious family, they are the one reason that makes me myself. I have learned what is hardship and how to be strong against wrong, especially from my mother Sedefiye TELLİ. She is the most faithful, thoughtful person I know.

TABLE OF CONTENTS

LIST OF TABLES

LIST OF FIGURES

LIST OF SYMBOLS AND ABBREVIATIONS

B	Bandwidth
BJT	Bipolar Junction Transistor
CAD	Computer Aided Design
CMOS	Complementary Metal-Oxide-Semiconductor
Cr:GaAs	Chromium Gallium Arsenide
DARPA	U.S. Defense Advanced Research Program Agency
dB	Decibel
dBm	Decibel with Milliwatt Reference
DC	Direct Current
FCC	Federal Communication Commission
FFT	Fast Fourier Transform
FWHM	Full Width at Half-Maximum
GaAs	Gallium Arsenide
GaP	Gallium Phosphide
GHz	Giga Hertz
GPR	Ground Penetrating Radar
HP	Hewlett-Packard
I_B	Base current
I_C	Collector current
IC	Integrated Circuit
I_E	Emitter current
InP:Fe	Iron-Doped Indium Phosphide
kHz	Kilo Hertz
kb/s	Kilobyte per second
MHz	Mega Hertz
MOS	Metal Oxide Semiconductor
MOSFET	Metal-Oxide-Semiconductor Field-Effect Transistor
nF	Nanofarad
NPN	N-type P-type N-type semiconductor
ns	Nanoseconds

OOK	On-Off Keying
PAM	Pulse Amplitude Modulation
PCB	Printed Circuit Board
PCSS	Photon Conductive Semiconductor Switching
pF	Picofarad
PN	P-type N-type semiconductor
PPM	Pulse Position Modulation
PRF	Pulse Repetition Frequency
ps	Picoseconds
RBW	Resolution Bandwidth
RF	Radio Frequency
Si	Silicone
SRD	Step Recovery Diode
TEM	Transverse Electromagnetic
UWB	Ultra-wideband
VBW	Video Bandwidth
V_{CE}, U_{CE}	Collector-Emitter voltage
V_{CEbr}, U_{CEbr}	Collector-Emitter breakdown voltage
V_{CC}	Positive supply voltage
VHF	Very High Frequency
μH	Microhenry
τ	Pulse width
n	Resistivity constant
M	Current multiplication factor
f	Frequency
τ_p	Full Width at Half-Maximum

1. INTRODUCTION

In this section, the background of short pulse generators, their applications, especially avalanche short pulse generators, and some key points to enlighten the design processes presented in this thesis are given.

1.1 Fundamentals of the Short Pulse Generators

Humanity has been utilizing UWB technology features for many years. In 1960, the sampling technology was invented by Hewlett-Packard (HP, now Agilent), and the company's first oscilloscope to use it (HP 185A) had a bandwidth of 500 MHz. HP 185A model oscilloscope is shown in Figure 1.1. This was a milestone, from this day forward the measurement and production of wider bandwidth signals were enabled. In 1962, bandwidth was increased to 1000 MHz with the HP 185B, this was going to be the first GHz oscilloscope (Anon 2022c).

Figure 1.1 Hewlett-Packard first sampling oscilloscope (HP 185A), 1960 (Anon 2022c).

Besides, the studies in electromagnetics in the time domain appeared in 1962 with the description and verification of analytical solutions on the transient behavior of the TEM-mode microwave networks through impulse response (Ross 1963, 1966). After the description and application of measurement with the impulse technique in wideband radiating antennas (Ross 1968), it became clear that short pulse radar and communications systems could be realized with the same perspective. Ross showed the usage of this technique in radar and communications at the Sperry Research Center (Bennett and Ross 1978). Sperry received the first UWB communications patent in April 1973 (Ross 1973). Until 1989, the UWB term was not used, instead this technology was referred to as baseband, carrier-free, or impulse by U.S. Department of Defense (Fontana 2002). The first definition of UWB technology dates back to the 1990s. The U.S. Defense Advanced Research Program Agency (DARPA) published the initial definition of UWB signals and systems in 1990 (Taylor 2012). Until the year 1994, the UWB technology was premature and was only used by U.S. Defense Agency for communications but later on, a huge acceleration has been made by all researchers and institutions. Some old applications that can be counted as the first applications of this technology were given in Figure 1.2 (Fontana 2002).

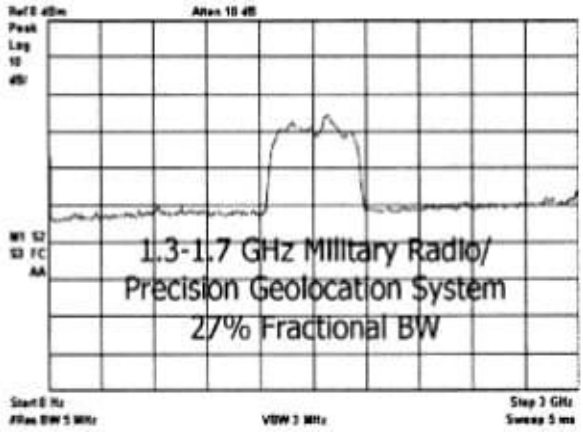

(a)

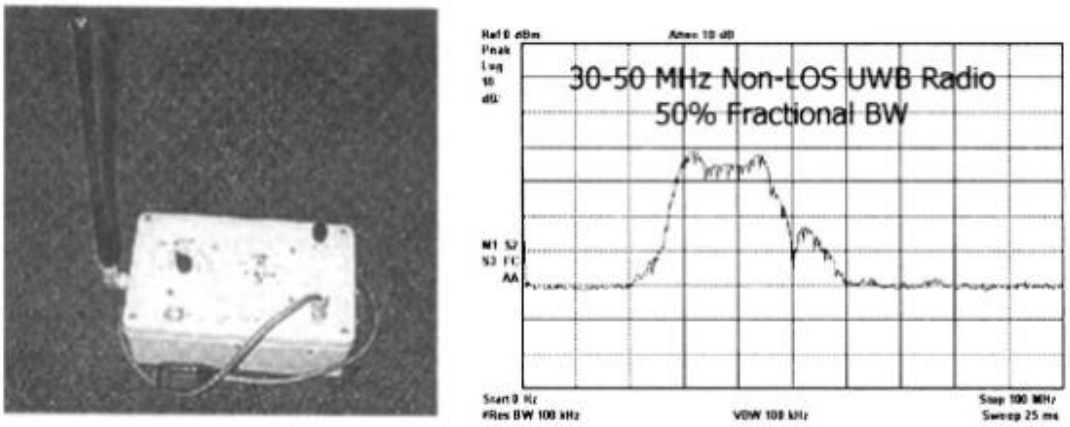

(b)

Figure 1.2 First applications of UWB technology. a) Full duplex UWB handheld transceiver, b) UWB groundwave communications system (Fontana 2002).

The device given in Figure 1.2(a) is a handheld transceiver that has a data transfer rate of 128 kb/s, and it has a center frequency of 1.5 GHz with 400 MHz instant bandwidth. Similarly, Figure 1.2(b) shows a groundwave communication system that has a data rate of 128 kb/s. That communication system could support 10 miles using a standard 30-88 MHz VHF military antenna. More information about applications can be found in the cited book chapter.

The other definition of the UWB term is done in 2002 by Federal Communication Commission (FCC). According to that definition, UWB is defined as a spread spectrum wireless communication system with a bandwidth at least 20% greater than the center frequency, or a bandwidth of 500 MHz or more (Federal Communications Commission 2002). In daily applications, UWB signals have a -10dB bandwidth from 3.1 GHz to 10.6 GHz. Other definitions are also available, but this is accepted by most of the application areas such as communications, wall-imaging systems, ground-penetrating radar systems (GPR), medical systems, and measurement systems. To reach up to that bandwidth, a signal generation with narrow pulse width is necessary as the Fourier transform explains (Bracewell and Bracewell 1986). These signal generators that have ability to generate pulses between 3.1 GHz and 10.6 GHz are called short or ultra-short pulse generators. Today, a wide range of applications such as UWB communications systems, remote sensing, GPR systems, and medical systems necessitate short pulse generators due to demand for high bandwidth. For communication systems, high bandwidth is equivalent to high data rate and increased

system security. For radar or imaging systems, it means increased resolution and better detection of desired objects.

After understanding the necessity of the shorter pulse generation and its impact on daily life, methods to reach this goal are examined by reviewing the literature. The short pulse generation primarily relies on the semiconductor device technology. As the first method to generate short pulses (nanoseconds or picoseconds), photon conductive semiconductor switching devices (PCSS) can be told. In this method, PCSS needs to be triggered by a short laser pulse which makes them conductive instantly thus an ultra-short pulsed current is created. Semiconductor materials such as GaAs, Si, Cr:GaAs, GaP, and InP:Fe can be used to form a PCSS. The second method to create a short pulse relies on the nonlinear switching characteristics of semiconductor devices. In this method, even though the devices are low power compared to the previous method, they have pros such as low power consumption, small size, and ease of integration and usage. Some components have been used in the creation of short pulses including avalanche transistors (Wang et al. 2009), tunnel diodes (Kamegai et al. 2008; Matiss et al. 2007), and step-recovery diodes (Protiva, Mrkvica, and Macháč 2010; Valizade, Rezaei, and Orouji 2017; Wong Choi, Joo Choi, and Hoon Han 2011) as an example of this method (Miller 1986). In general, step-recovery diodes and tunnel diodes generate pulses having widths varying from several picoseconds to hundreds of picoseconds with amplitude of hundreds of millivolts, while avalanche transistors create pulses having widths of hundreds of picoseconds and amplitude of tens of volts (Wang et al. 2008).

Because of the requirement for generators with narrow pulse width, high precision, high power, and high bandwidth, research on the short pulse demanding fields is becoming more and more popular. Semiconductor devices using the avalanche effect are one of the research areas to reach these goals. The recent studies mention the avalanche transistors as a more powerful and stable pulse creation technique compared to others (Wang et al. 2008). The term avalanche transistor in this thesis refers to a transistor operated in avalanche mode.

1.2 Literature Survey of The Avalanche Short Pulse Generators

Avalanche transistors were used to create a monocycle pulse in 1994 by M. Morgan (Morgan 1994). They are supplied by a high voltage source to create a strong electric field to operate in avalanche mode (Oppermann, Hämäläinen, and Iinatti 2004). The avalanche transistors are low cost and provide large amplitude pulses with a narrow pulse width at the output compared to other nonlinear pulse generators. They are stable, have long life, and are quick to react to trigger signals. They present ease in triggering and driving processes (Wang et al. 2008; Wang, Zhang, and Shi 2020; Wu and Tian 2010). Numerous applications those involving ground-penetrating radar (GPR) (Omurzakov, Keskin, and Turk 2016; Wang et al. 2020), UWB communications (Wang et al. 2008), etc. require these characteristics. For radar applications, the aforementioned properties suggest higher resolution and better imaging, while for UWB communications, high data-rate and increased security. Numerous studies for applications involving quick switching and short pulse creation have recently been published.

Some avalanche short pulse generator designs have single or multiple transistors with trigger circuits and signals, and a number of multi-transistor designs employ cascaded or series-connected transistor topologies (Omurzakov et al. 2016; Wang et al. 2020). Some short pulse-generating designs include pulse-shaping circuits just before the output. Thus there are pulse-creating and shaping designs using avalanche transistors together with SRDs described in (Guo and Zhu 2014; Yin, Pan, and Zhang 2018). As can be understood from referred studies, short pulse generators using avalanche transistors carry the properties that can meet the mentioned requirements of the areas such as radar systems (Ahajjam et al. 2020; Ameri, Kompa, and Bangert 2011; Sim, Kim, and Hong 2009; Wang et al. 2020; Xia et al. 2013), UWB communications systems (Arafat and Harun-ur-Rashid 2012; Razavi et al. 2005; Wang et al. 2008), and many others.

Avalanche pulse generators are widely discussed in the literature. One study uses multiple transistors including trigger circuitry (Omurzakov et al. 2016). In order to make the transistor avalanche, such systems include a complex trigger circuitry and a high dc voltage (375V).

The primary design objective of this thesis was to develop a novel and simple circuit topology that was distinct from those described in the literature, and to produce a small pulse width and high-power level at the output suitable for radar systems, UWB communications systems, etc.

The second aim for this study is to control the pulse width and pulse amplitude of the generated pulse. For example, in imaging systems (wall-imaging, ground-penetrating radar, etc.) high precision is required to detect and image smaller objects. And for this reason, higher frequencies or shorter wavelengths are desirable. On the other hand, larger wavelengths or lower frequencies are needed to detect and image larger objects. Thus, a system with controllable pulse width can achieve detection and fine imaging of the object. And high amplitude pulses are desired to penetrate thicker walls or obstacles. Before going into the individual parts of the avalanche pulse generator, some basic theories and design goals are given. As an external requirement, a dc power supply design is explained in detail.

2. MATERIALS & METHODS

In this section, the basic theory of the avalanche effect phenomenon, short pulse creation through avalanche method, frequency mixing, and their use in this thesis are explained. The power supply circuit topology that is required to power the avalanche pulse generators is also provided.

2.1 Avalanche Effect

Avalanche breakdown or avalanche effect is one of the breakdown mechanisms that is observed in Zener diodes and transistors. The other mechanism is the Zener breakdown which is out of the scope of this study. A voltage referred to as breakdown voltage occurs as a result of these two different breakdown mechanisms and it varies from 2V to 2000V in general, 20V to 1000V for the MOSFETs (Horowitz, Hill, and Robinson 1989). An instant increment happens in the current flowing through mentioned material types when they are under high electrical force.

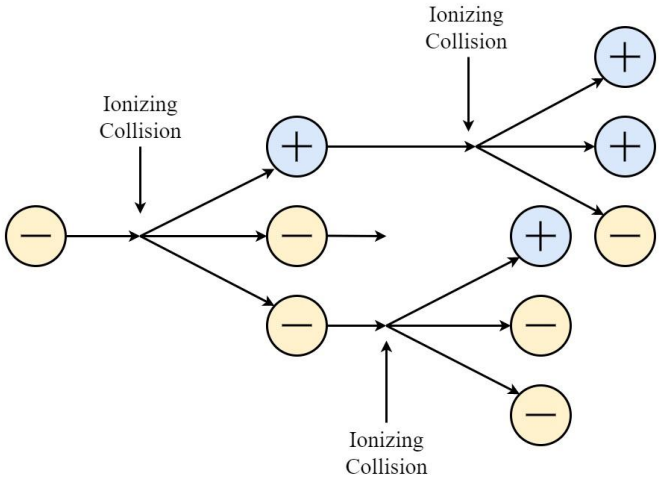

Figure 2.1 Impact ionization in avalanche breakdown process (Jaeger and Blalock 1997).

As an example of semiconductors, silicon diodes with breakdown voltages greater than about 5.6V enter the breakdown via an avalanche breakdown mechanism. The electric field increases as the width of the depletion layer increases in the PN junction under reverse bias. When the reverse bias voltage is sufficiently high, free carriers in the depletion region are accelerated, they move through the depletion region and collide with fixed atoms. At some point, the electric field and the width of the space charge region become large enough that some carriers gain enough energy upon impact to break covalent bonds, resulting in electron-hole pairs. Through this impact-ionization process, the new carriers created can also accelerate and create additional electron-hole pairs, as shown in Figure 2.1 (Jaeger and Blalock 1997). In this manner, considerable amounts of crystals that are insulators typically become electrically conductive due to impact ionization. And this sudden increase in current flowing through a crystal can be used for short pulse creation.

For the avalanche transistors, as the main focus of this thesis, same logic is valid. However, the working principles of the transistors are slightly different than diodes.

Transistors have four different operating regions referred as saturation, linear, cut-off, and avalanche regions. The emitter junction of an NPN transistor is forward-biased when a positive current ($I_B>0$) is introduced into the base. On the contrary, if a negative current ($I_B<0$) is introduced into the base, the emitter junction is reverse biased.

i. For the linear region, collector current I_C and base current I_B change linearly with one another.

ii. For the saturation region, collector current I_C does not exhibit any variation with the base current I_B.

iii. A cut-off region is one where the base current I_B equals to zero.

iv. An avalanche region is one where the collector current I_C varies substantially in a short period of time when the base current I_B is negative.

The 4th statement takes place because of the multiplier effect in avalanche transistors. When a strong electric field is created by applying a high collector voltage, electrons in the depletion region accelerate because of the reverse bias ($I_B<0$), similar to in the diode case (Wang et al. 2008). In Figure 2.2, I_C curve characteristics upon the different collector-emitter voltages (V_{CE} or U_{CE}) of avalanche transistors are given.

In this thesis, short pulses were created through the avalanche effect phenomenon of the BJTs. As explained before, NPN BJTs were supplied with high voltage at their collector terminals. The current in the collector-emitter junction increases greatly by a current multiplication factor (*M*) due to avalanche. The current multiplication factor *M* is given in Equation 2.1 for BJTs. Here "*n*" is the resistivity constant of the transistor ranging from 2 to 10.

$$M = \frac{1}{1-\left(\frac{V_{CE}}{V_{CEbr}}\right)^{n}} \tag{2.1}$$

When a transistor works in the avalanche mode, it shows the following characteristics:

i. The current gain of the transistor in the linearity region multiplies with the current multiplication factor (*M*).

ii. The cut-off frequency goes high.

iii. Negative resistance characteristics are shown in the collector-emitter junction.

iv. A pulse created through this effect is dependent on the bias voltage, charged capacitor, and load resistor in terms of output pulse amplitude and pulse width.

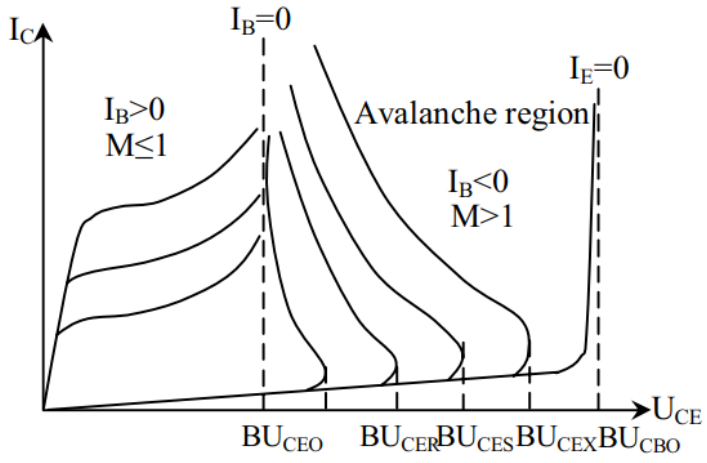

Figure 2.2 I_C versus V_{CE}(or U_{CE}) curve to show avalanche region characteristics (Wang et al. 2008).

2.2 Pulse Shortening due to Mixer Effect

Mixers are nonlinear devices that have two inputs and one output; mixer translates the frequencies at its inputs to sum and difference frequencies at its output. The mixer function is mostly named multiplication of frequencies. Sums and differences are the products of this multiplication (Davis and Agarwal 2003). By considering equi-amplitude sinusoidal signals $A(t)$ and $B(t)$, where $A_0(t) = B_0(t)$ that are input to a mixer and $Y(t)$ is the output of the mixer, following Equations can be written to represent the optimal mixer operation (Chang, Nair, and Bahl 2001; Vendelin et al. 2021).

$$A(t) = A_0(t)\, cos(\omega_1 t) \tag{2.2}$$

$$B(t) = B_0(t)\, cos(\omega_2 t) \tag{2.3}$$

$$Y(t) = A(t) \times B(t) = \frac{{A_0}^2(t)}{2}\{cos[(\omega_1 + \omega_2)t] + cos[(\omega_1 - \omega_2)t]\} \tag{2.4}$$

Since a mixer carries out signal multiplication process, let's find out what happens if two identical Gaussian pulses are multiplied instead of sinusoidal signals. MATLAB simulations are performed to answer this question. Here in Figure 2.3, an example Gaussian pulse with 1.06ns pulse width and 1V pulse amplitude is shown. Its frequency spectrum extends to a little bit more than 1 GHz and its magnitude is normalized to 1 by dividing its own maximum value. The approximation of Gaussian pulse expression is given with the equation below where τ_p is full width at half-maximum (FWHM) pulse duration. Now, let's apply Gaussian-shaped pulses to the mixer inputs. Equations 2.5 and 2.6 represent identical Gaussian pulses that are input to a mixer, and Equation 2.7 represents the output of the mixer due to mixer multiplication operation.

$$A(t) = A_0 e^{-2ln_2 \frac{t^2}{\tau_p^2}} \tag{2.5}$$

$$B(t) = A(t) \tag{2.6}$$

$$Y(t) = A(t) \times B(t) \tag{2.7}$$

Let's assume that the mixer inputs are $A(t)$ and $B(t)$ where $A(t)$ is given by Equation above and $B(t) = A(t)$. So the mixer has two identical Gaussian inputs. Using MATLAB, $A(t)$ (and also $B(t)$) is plot and shown in Figure 2.3(a). Spectrum of $A(t)$ is obtained through Fast Fourier Transform (FFT) and denoted as $A(f)$ which shown in Figure 2.3(b).

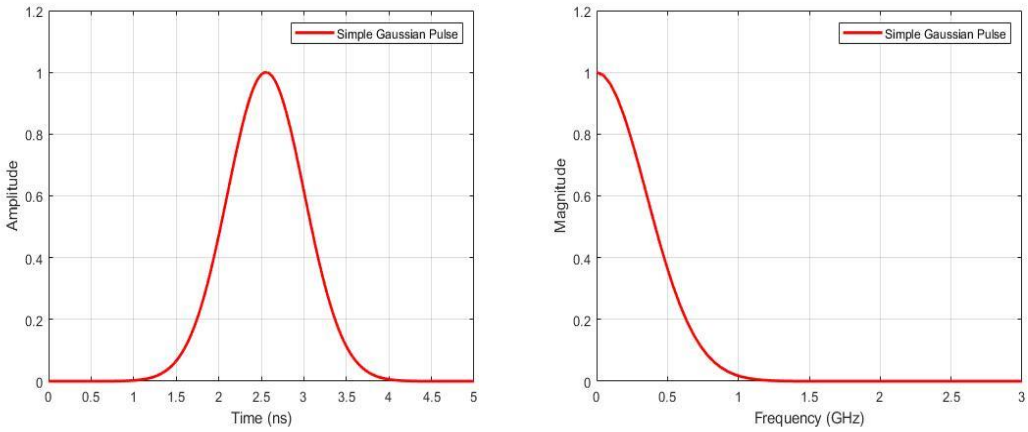

(a) **(b)**

Figure 2.3 (a) Simple Gaussian pulse $A(t)$, and (b) its spectrum $A(f)$.

Figure 2.4(a) shows the comparison of input Gaussian pulse $A(t)$ and output Gaussian pulse $Y(t)$ which is obtained through multiplication process of $Y(t) = A(t) \times B(t)$ where $B(t) = A(t)$. It can be seen that the input and output Gaussian pulses have pulse widths of 1.06 ns and 0.75 ns, respectively. And that corresponds to about 30% shorter pulse width at the output of the mixer. Figure 2.4(b) shows the spectrums of input and output Gaussian pulses $A(f)$ and $Y(f)$, respectively. And it can be seen that the output spectrum of the mixer extends up to about 1.51 GHz. And that corresponds to about 41% wider bandwidth at the output of the mixer compared to its input. In summary,

mixer or the multiplication process generates sum and difference frequencies, harmonics of the input frequencies and the original frequencies. So the output of a mixer appears quite rich in spectrum as opposed to its input. This rich spectrum can also be described as broadened or widened. Since the mixer operation results in broadening the spectrum, it can be said that it also results in shortened pulse width as shown in Figure 2.4(a). This is because wider spectrums are due to narrower pulse widths through Fourier transform. In Figure 2.4, normalized values of the Gaussian pulses are used for time domain and frequency domain representation. The values in the time domain vector of the Simple Gaussian Pulse and Output of Mixer are divided by their own maximum element hence, the maximum value is limited to 1 and all values are normalized according to 1 as shown in Figure 2.4(a). As the same, Gaussian pulse values are transformed into the frequency domain and they are normalized according to their own maximum values as shown in Figure 2.4(b). The spectrums and the time domain representations were normalized since pulse properties, spectrum, and magnitude relation is seen better in this case. This process was done just for demonstration since pulse widths and spectrum widths are not changing with this modification.

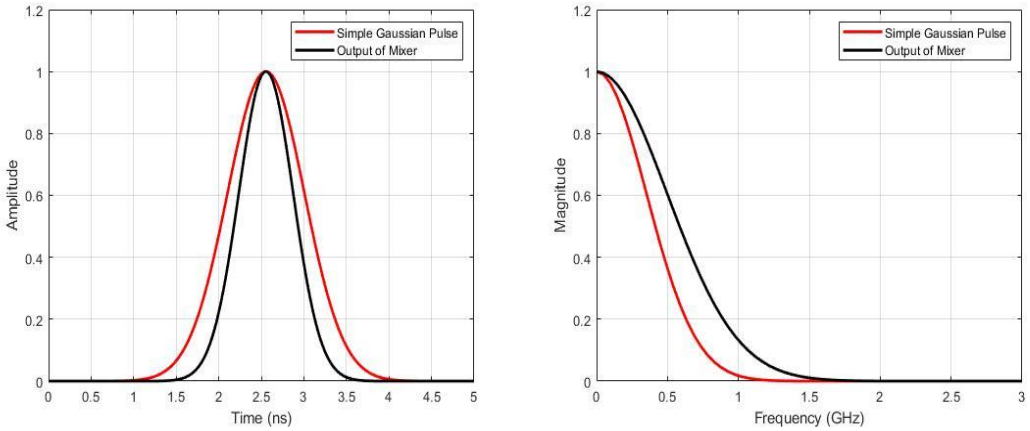

Figure 2.4 (a) Time domain comparison of Gaussian pulse A(t) and Output of Mixer $Y(t)$. (b) Frequency domain comparison of $A(f)$ and $Y(f)$.

As can be seen from Figure 2.4, mixer operation narrows the pulse width and enhances the bandwidth. A mixer is a nonlinear device or circuit. Nonlinearity can be modeled by the Taylor series given in Equation below (Pozar 2011).

$$v_o(t) = \alpha_0 + \alpha_1 v_i(t) + \alpha_2 v_i^2(t) + \alpha_3 v_i^3(t) + \alpha_4 v_i^4(t) + \cdots \quad (2.8)$$

So, applying these identical Gaussian pulses $A(t)$ and $B(t)$ to the nonlinearity equation of (2.8) through $v_i(t)$ by setting $v_i(t) = A(t) + B(t)$ and assuming $\alpha_0 = 0$ and the coefficients $\alpha_k = 1$ for $k = 1,2,3,4,\ldots$ results Figure 2.5. The time domain and frequency domain outputs of the nonlinear device are symbolized by $v_o(t)$ and $v_o(f)$ respectively.

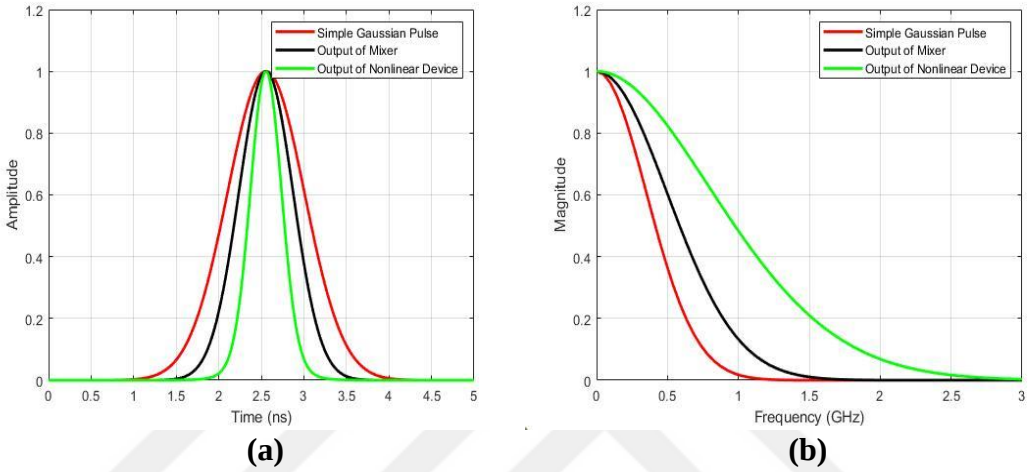

Figure 2.5 (a) Time domain comparisons of all operations ($A(t)$, $Y(t)$, $v_o(t)$) (b) Frequency domain comparison of all operations ($A(f)$, $Y(f)$, $v_o(f)$).

As explained the mixer effect generates harmonics, sum and difference frequency components at the output due to second order nonlinearity and Figure 2.4 shows only the time domain multiplication products of the two identical signals. In reality, a nonlinear device or circuit may exhibit nonlinearities higher than two. To observe these effects, input signals are applied to Equation (2.8) up to the 7th order nonlinear term. And it is shown that the pulse broadening effect due to nonlinearity is real. Figure 2.5(a) shows three pulses; a simple Gaussian pulse at the input of a mixer or a nonlinear device, output pulse due to mixer, and output pulse due to nonlinear device. Figure 2.5(b) shows the corresponding spectrums. It can be observed that as the degree of nonlinearity increases, spectrum of the output pulse broadens, and the pulse width shrinks in time domain. In Figure 2.5(a) and (b), comparisons of all the operations in the time domain and frequency domain are given respectively. While they represent the operations' results, their outputs are normalized according to 1 by dividing them by the maximum value in their own time vector. Also, after the time domain values

were converted to frequency values to see their spectrum they are normalized to 1 as well for better visualization.

The results of all simulations are given in the Table 2.1 to compare in terms of bandwidth and pulse width. Here it is obvious that the expectation of enhancement in bandwidth is achieved by using this method.

Table 2.1 The results of all operations

Pulse	Bandwidth (GHz)	Pulse width (ns)
Simple Gaussian Pulse $A(t)$	1.07	1.06
Output Pulse due to Mixer Operation $A(t) \times B(t)$	1.51	0.75
Output Pulse due to Nonlinearity Equation	2.68	0.44

Here the bandwidth is accepted to be the frequency value at the %1 of maximum power shown by the spectrum and pulse width is the time axis difference shown at the %50 of pulse amplitude.

2.3 Design of the Power Supply

Thanks to the inherent property of the avalanche effect, which is explained in section 2.1, it is possible to design short pulse generators using avalanche effect of the transistors if a high dc voltage supply is designed and built. Thus, a high-voltage power supply is needed to be designed to operate pulse generator circuits. Such a power supply was designed using a 555 IC (Anon 2022a) and a suitable MOSFET. 555 IC was used to generate a square waveform whose duty cycle can be varied by an external potentiometer. Pulses produced by 555 IC are fed to the gate of the IRF840 MOSFET (Anon 2021) and turns it ON and OFF. An inductor at the drain of the MOSFET is used to charge a capacitor to dc voltage through a rectifier diode. The feedback stage includes LM358P Op-Amp (Anon 2022b) and PN2222A BJT (Anon 2004) and works as the comparator between the external potentiometer and output voltage to arrange and keep the voltage level stable. This circuit is energized by a basic +12V dc supply.

The output is a dc which varies from 30 to 300V. The high-voltage dc power supply circuit block diagram is given in Figure 2.6. Also, the printed circuit board (PCB) of the power supply circuit can be seen in Figure 2.7.

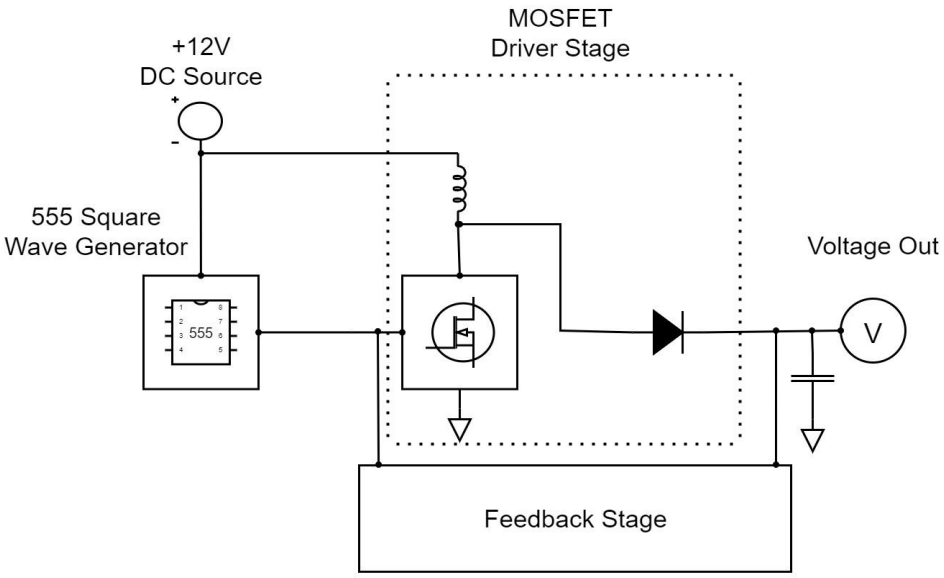

Figure 2.6 Circuit block diagram of the dc power supply.

Figure 2.7 Manufactured dc power supply.

3. ASSESSMENT OF THE FINDINGS

3.1 Single and Double Transistor Avalanche Pulse Generators

In this section, before proceeding with the designs and measurements of single and double-transistor avalanche pulse generators, the system topology that is imagined to enhance the bandwidth and narrow the pulse width using the aforementioned theories is proposed. This section continues with the design of a single-transistor base circuit its measurements and the double-transistor circuit which will show the mixer effect.

3.1.1 Key Points of System Topology

As we understand from sections 2.1 and 2.2, using the avalanche effect, the creation of a Gaussian-shaped short pulse is possible, and theoretically broadening the spectrum through the mixer effect could be helpful to reach one of the desired goals for this thesis. Therefore, a new circuit topology is imagined and proposed.

The suggested circuit consists of two identical avalanche pulse generators driving the same 50-Ω load. The pulse spectrum is assumed to get wider by utilizing the mixing effect of the avalanche transistors. As a consequence of the wider bandwidth, the output pulse width is decreased. The avalanche pulse generator circuit that is being suggested is going to be an improved, novel version of the basic one-transistor circuit (Chadderton 1996). In Figure 3.1, the suggested circuit topology is displayed. We used measurements rather than simulations to construct our circuits because the available Spice models do not incorporate the avalanche multiplication mechanism reliably. However, a novel and straightforward approach was created in (Dias 2005) to take the avalanche effect into account.

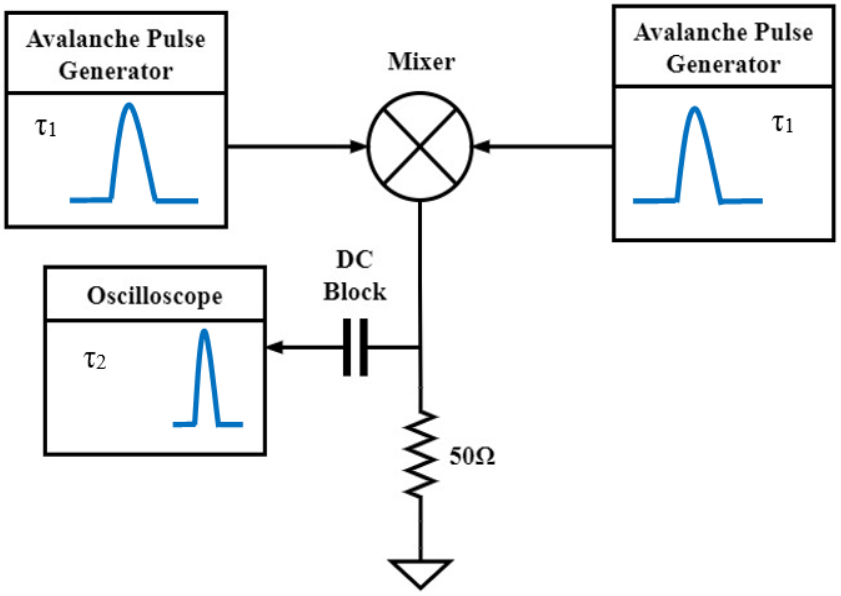

Figure 3.1 Block diagram of the proposed circuit.

Figure 3.1 depicts the block diagram of the proposed pulse generator circuit, which consists of two identical avalanche pulse generators driving a single 50-Ω load resistor and a mixer. As it is explained in 2.2, theoretically, when two signals are applied to the mixer, sum and difference frequencies and the harmonics of the input signals are seen at the output. Given that the mixer behaves nonlinearly and the input signals are assumed to be identical Gaussian-type pulses, the output signal ought to have a larger bandwidth than the bandwidth of a single input pulse. According to the Fourier transform, a wider spectrum results in shorter pulse width in the time domain.

Consequently, the output pulse width τ_2 must be less than τ_1 when the input signals are identical and have a pulse width of τ_1. An appropriate filter can be used to correct any distortion in the output pulse waveform. One other objective of this thesis objective is to illustrate this effect by introducing new circuit designs.

As a starting point to reach the proposed circuit designs and show up the effects desired, we shall proceed with the basic avalanche pulse generator circuit in section 3.1.2.

3.1.2 Single Transistor Base Circuit Design

The first step of this study is to make up a primary avalanche pulse generator with desired properties. The preferred properties of the short pulse generators can be listed as compactness, simplicity, being easy to trigger, and generation of the positive narrow pulse in the time domain as explained in section 1.2. To this end one-transistor basic avalanche pulse generator is created. This circuitry does not require any trigger signal and complex trigger circuit differently from its equivalent circuits in the literature. Moreover, it provides a positive high amplitude output pulse and narrow pulse width.

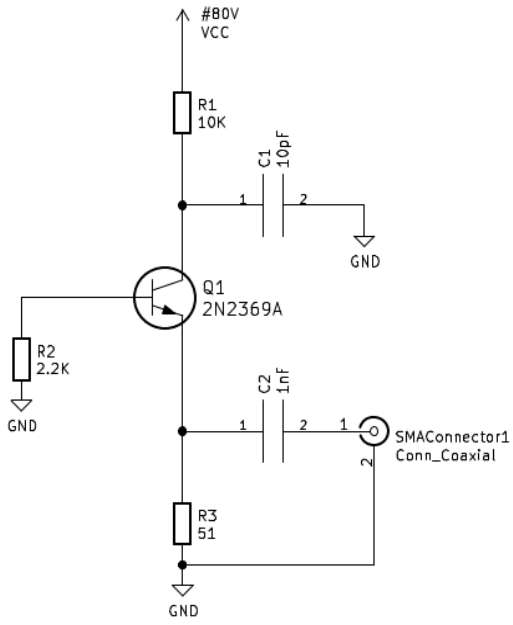

Figure 3.2 Circuit schematic of the the single-transistor self-triggered avalanche pulse generator.

In Figure 3.2 circuit schematic of the one-transistor pulse generator circuit is given. The schematic includes a 2N2369A transistor as the active device (Anon 2014). Initially, there have been many trials to optimize values of C1 and R1 then the values were selected as 10pF and 10KΩ. C1 is charged by high dc voltage V_{CC} through R1. V_{CC} has been increased slowly when it got closer to the avalanche breakdown voltage level. When the V_{CC} reaches the avalanche breakdown voltage, Q1 enters avalanche

mode and discharges the charged C1 rapidly. The discharge current of C1 generates a Gaussian-shaped short pulse that is taken from R3 via the output capacitor C2. When V_{CC} reaches 80V, the one transistor base circuit is in the avalanche mode and is referred to as a self-triggered avalanche pulse generator because of the reason that the base terminal of Q1 is not driven by any external signal and is grounded via R2. Also, the output signal is taken from the emitter terminal to obtain a positive pulse.

For the circuit shown in Figure 3.2 and all other circuits presented in this thesis, a 300 MHz digital oscilloscope (Rigol Tech. DS2302A) was used to measure the time domain response, and a 30 GHz spectrum analyzer (Rohde&Schwarz FSV3030) was used to measure the frequency domain response. For more accurate measurements, a high bandwidth oscilloscope would be better. However, since it is not available, a 30 GHz spectrum analyzer was used to observe the pulse broadening effect accurately instead of measuring the pulse width accurately.

The time domain output of the measured pulse is demonstrated in Figure 3.3(a). The values of pulse width and pulse amplitude were respectively 1.38ns and 7.12V. The output pulse spectrum of the single-transistor pulse generator circuit is shown in Figure 3.3(b) and the difference shown with the noise floor is presented. In this measurement, an external dc block which is up to 6 GHz was used to connect the PCB board to the spectrum analyzer device and the internal attenuation was set to 0-dB. The device's resolution bandwidth (RBW) and video bandwidth (VBW) were set to the values 3 MHz and 300 kHz respectively. And for each measurement included in this thesis, these configurations remained the same. At roughly 7.5 GHz, the output pulse spectral energy eliminates completely, as seen in Figure 3.3(b).

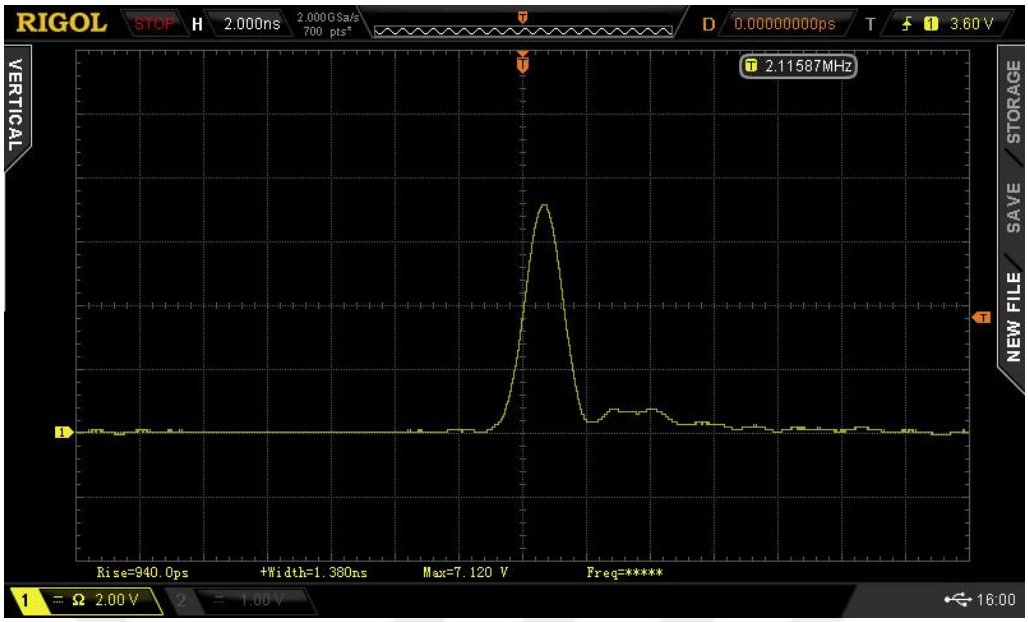

(a)

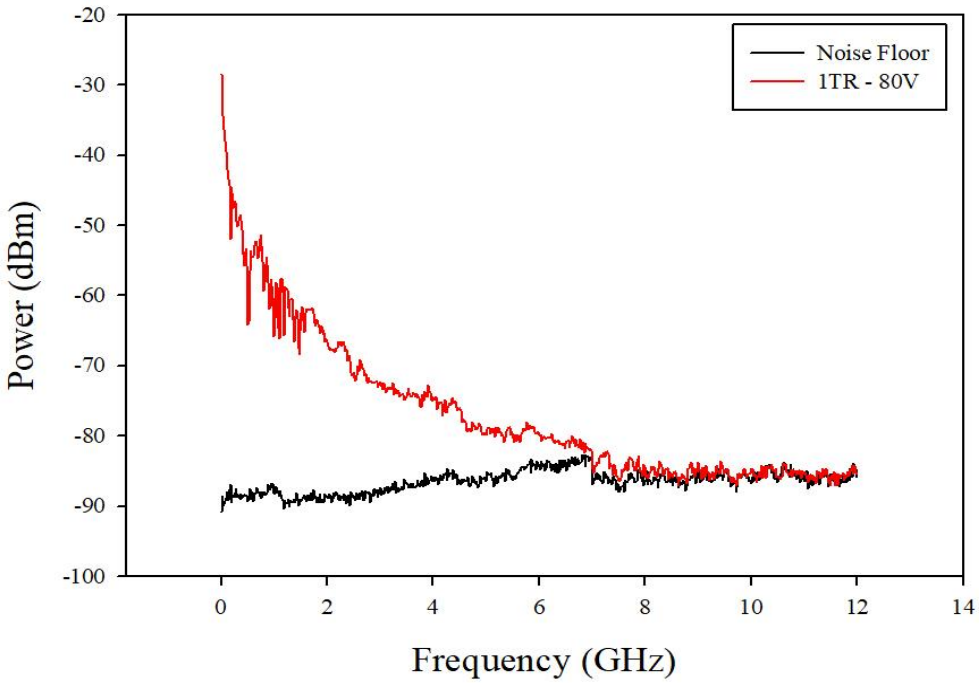

(b)

Figure 3.3 (a) Output pulse in time domain, and (b) in frequency domain, for the single-transistor self-triggered avalanche pulse generator.

3.1.3 Dual-Transistor Circuit Design

The base circuit depicted in Figure 3.2 was enhanced with the addition of another transistor as shown in Figure 3.4(a). Through the base resistors R3 and R4, both transistors are in self-triggered mode. Initially, V_{CC} was adjusted to 80V, just like in the circuit with a single transistor. A common load resistor, R5, is driven by transistors Q1 and Q2. The manufactured circuit is shown in Figure 3.4(b).

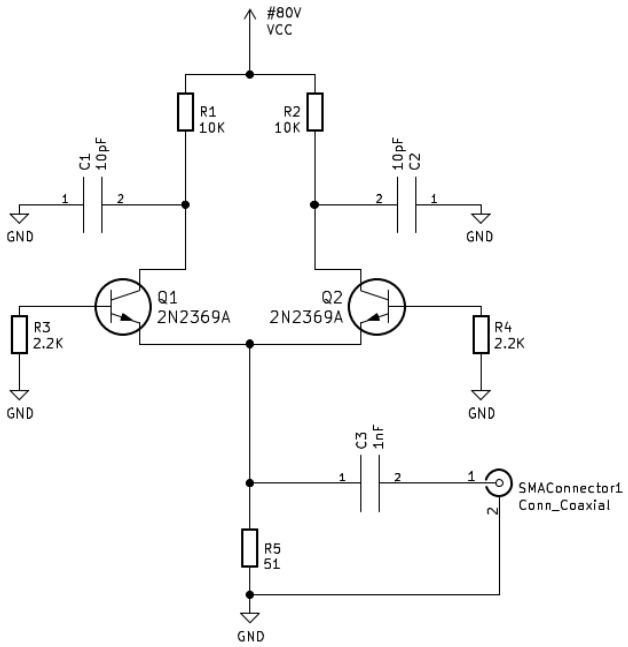

a)

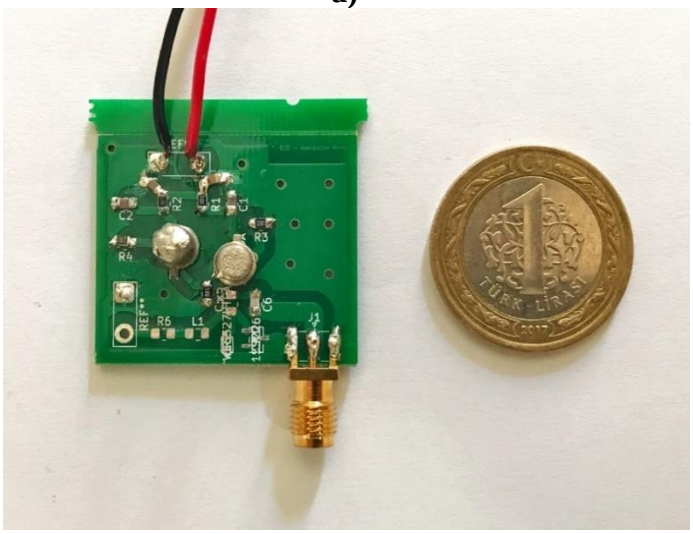

b)

Figure 3.4 (a) Schematic of the dual-transistor avalanche pulse generator. (b) Photograph of the manufactured circuit.

The output pulse is displayed in the time domain in Figure 3.5(a). Pulse width and pulse amplitude were measured. The measured pulse parameters were 1.24ns and 17.40V, respectively. In Figure 3.5(b), the measured pulse spectrum is displayed. As can be seen, the output of the spectrum power is greater than the single-transistor base circuit and the pulse spectral energy is around 6 dB higher than the noise floor at 12 GHz.

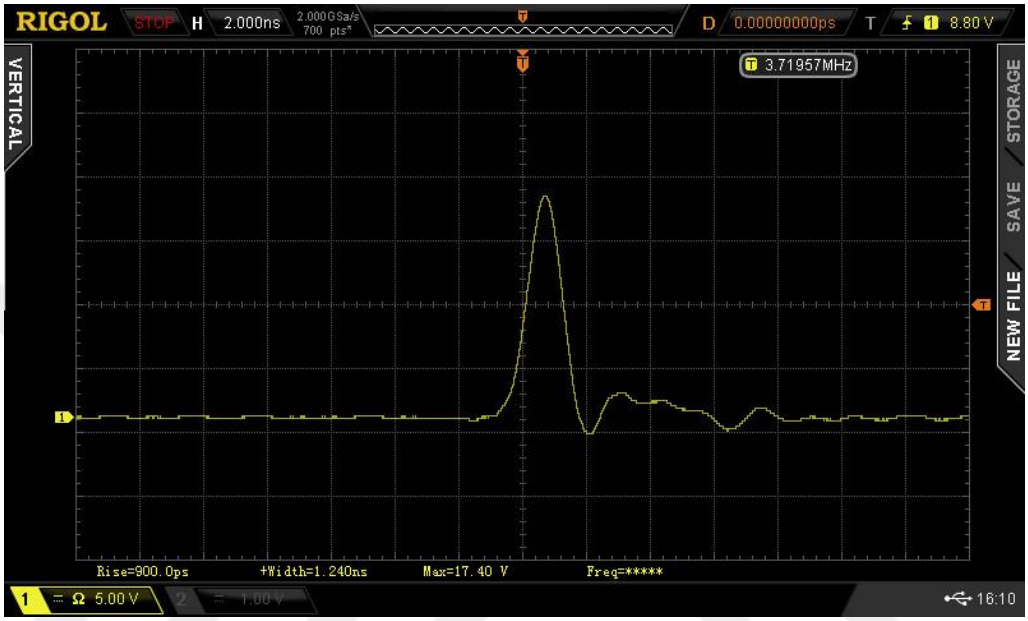

a)

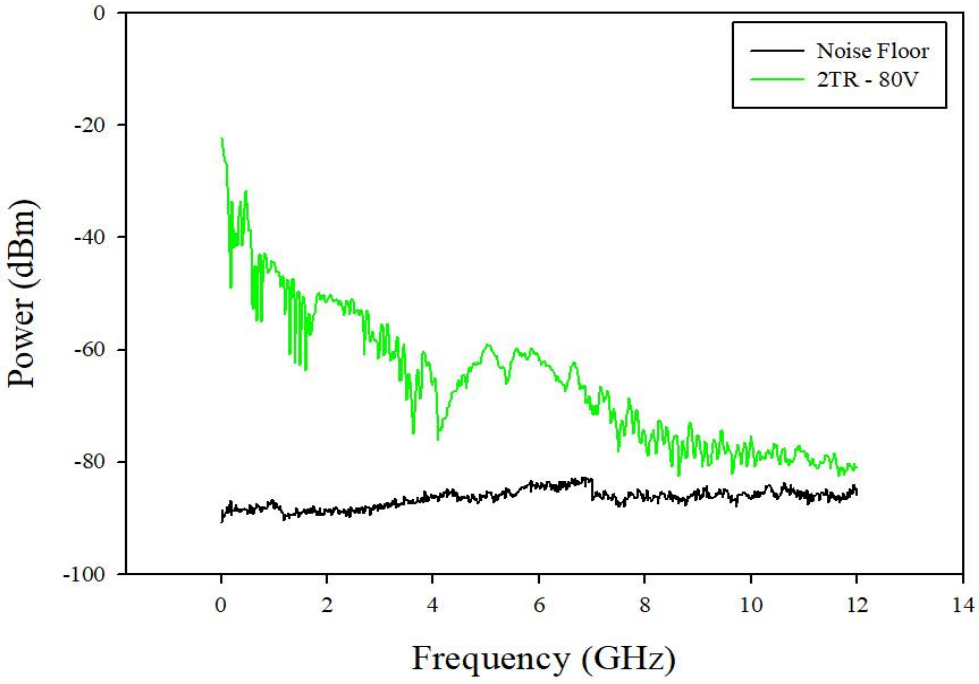

(b)

Figure 3.5 (a) Output pulse in time domain, and (b) in frequency domain of the dual-transistor avalanche pulse generator.

Figure 3.6 depicts the comparison of the pulse spectrums of single and dual-transistor cases when V_{CC} was set to 80V. The output spectral power seen is approximately 16 dB higher at 3 GHz, approximately 18 dB higher at 6 GHz, and approximately 8 dB higher at 9 GHz. As can be seen, some spectral energy remains at around 12 GHz. The mixing of the two output pulses by Q1 and Q2 could explain the broadening of spectral energy. Despite the fact that the 2N2369A is a non-RF BJT, the circuit shown in Figure 3.4 achieves bandwidth enhancement and power amplification without the use of a separate broadband power amplifier.

The claimed 80V supply voltage for UWB applications could appear implausible. However, since extremely low currents are enough for the avalanche activity, this voltage may readily be produced utilizing a very small power supply on the circuit board.

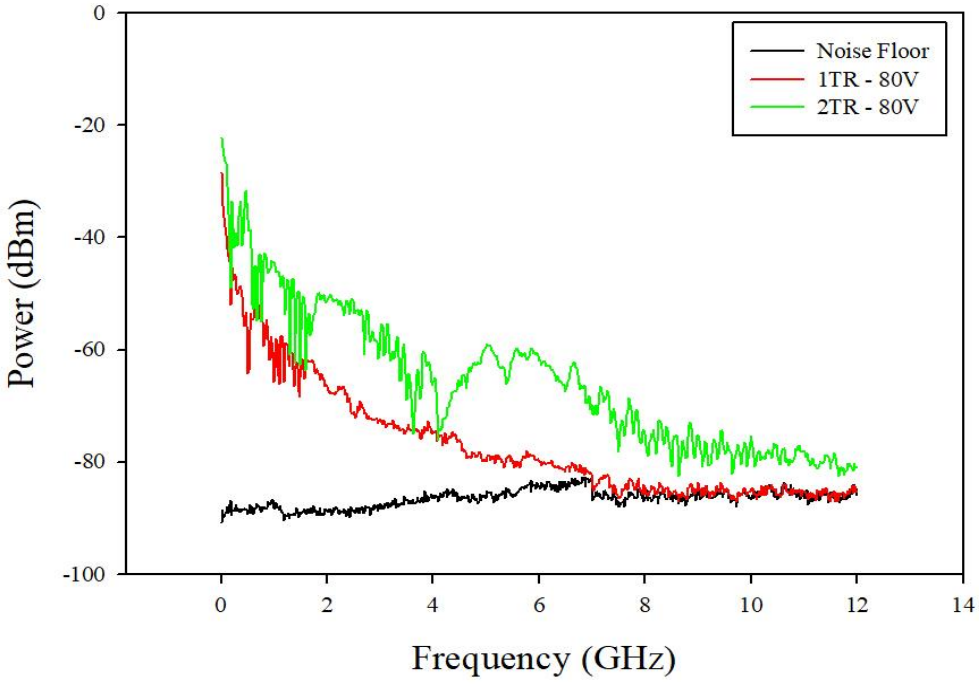

Figure 3.6 Comparison of spectrums of the single-transistor base circuit and the dual-transistor circuit.

3.2 Avalanche Pulse Generator with a Diode Mixer

After the observation of bandwidth, pulse width and pulse amplitude enhancement of the mixer effect of the double-transistor circuit, a passive diode mixer at the output of the circuit was tried for further improvement. The purpose here is to use a mixer stage to mix the signals generated by the avalanche transistors.

3.2.1 Single Transistor with Diode Mixer Circuit Design

A novel circuit topology was designed to decide if there is a mixing effect or not when only one mixer diode without a second transistor is placed at the output of the single-transistor base circuit as given in Figure 3.7. The avalanche mode is activated when V_{CC} reaches 80V. The diode which is tested to show mixing effect D1 (BAT15-03W) (Anon 2018) is connected in parallel with the load resistor R3 through a coupling capacitor C2. The diode D1 is forward-biased through an RF choke L1 and a current-limiting resistor R4. The bias voltage was selected at about 1.2V to overcome the 0.7V diode threshold voltage. The objective here is to create a short pulse using the avalanche effect, and then use the mixer diode D1's nonlinearity to create harmonics of the input pulse.

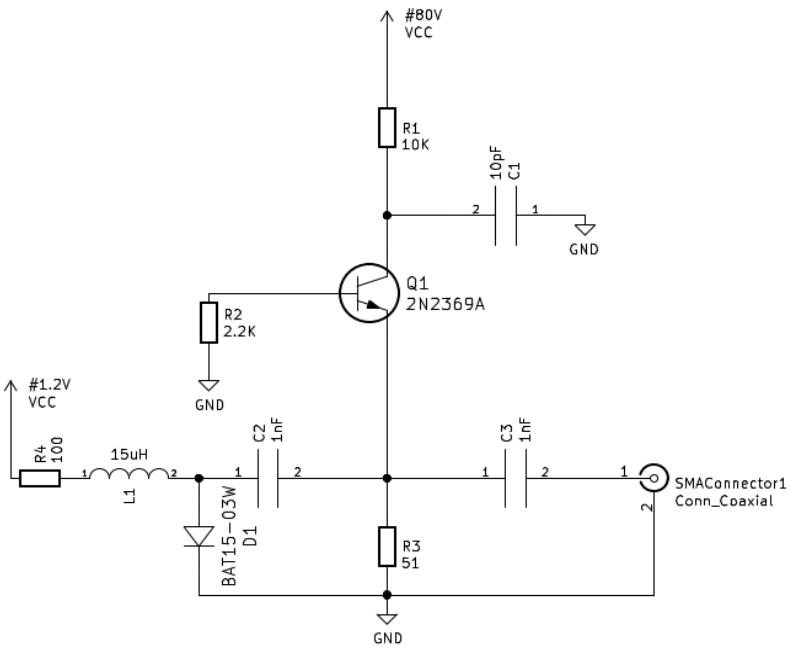

Figure 3.7 Schematic of the single-transistor avalanche pulse generator circuit with a diode mixer.

Figure 3.8(a) depicts the output pulse waveform of the circuit given in Figure 3.7. In Figure 3.8(b), the output spectrum demonstrated and compared with the 1TR – 80V case. As can be seen, the pulse width and pulse amplitude were depicted as 1.46ns and 5.56V, respectively. By checking the Figure 3.8(b), pulse spectral energy diminishes at about 7 GHz absolutely in both cases. The expectation about the spectral bandwidth was to see a slight improvement. The results demonstrate that adding a diode mixer to the single-transistor base circuit did not increase the spectrum enlargement. This might be because the diode mixer is passive element.

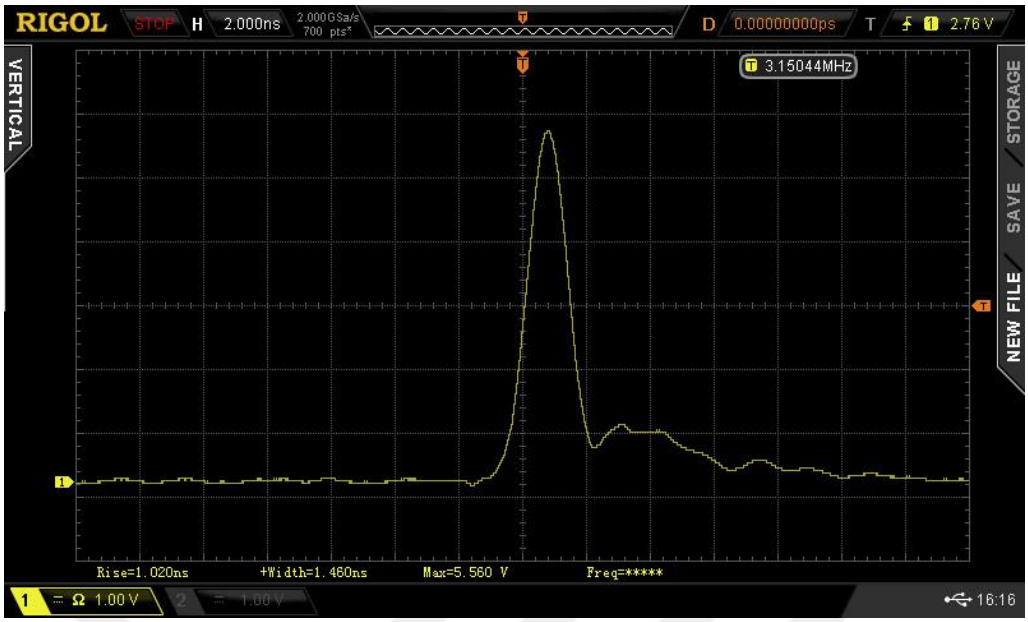

a)

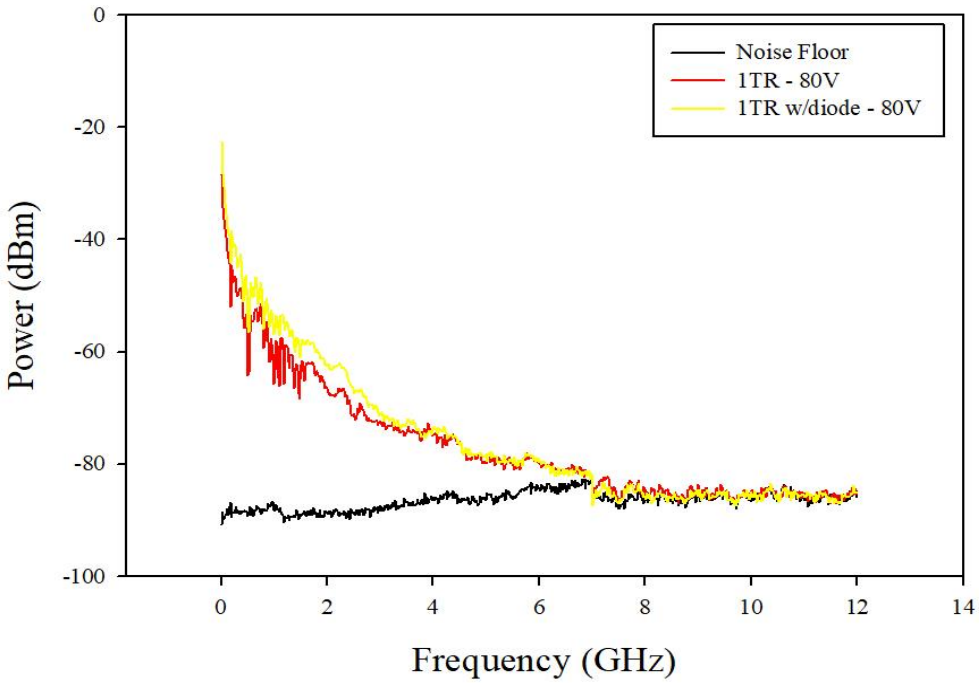

b)

Figure 3.8 (a) Output pulse in time domain, and (b) output pulse spectrum of the base circuit with diode at the output for V_{CC}=80V.

3.2.2 Dual-Transistor with Diode Mixer Circuit Design

As the following step in this work, two avalanche pulse generators composed of two 2N2369A transistors combine in parallel through a common load resistance (R5) as depicted in Figure 3.9(a). A mixer diode D1 (BAT15-03W) is connected in parallel

with the load resistor via a coupling capacitor C3 in the circuit. The mixing process is carried out by the diode. Through L1 and R6, it is forward biased. The bias voltage is around 1.2V. Both pulse generators are configured to operate in self-triggered avalanche mode. V_{CC} was set to 80V, the same as in the dual-transistor circuit. The purpose here is to build a broadband spectrum by combining two comparable pulses generated by each 2N2369A via the mixer diode. The printed circuit board which were manufactured is shown in Figure 3.9(b).

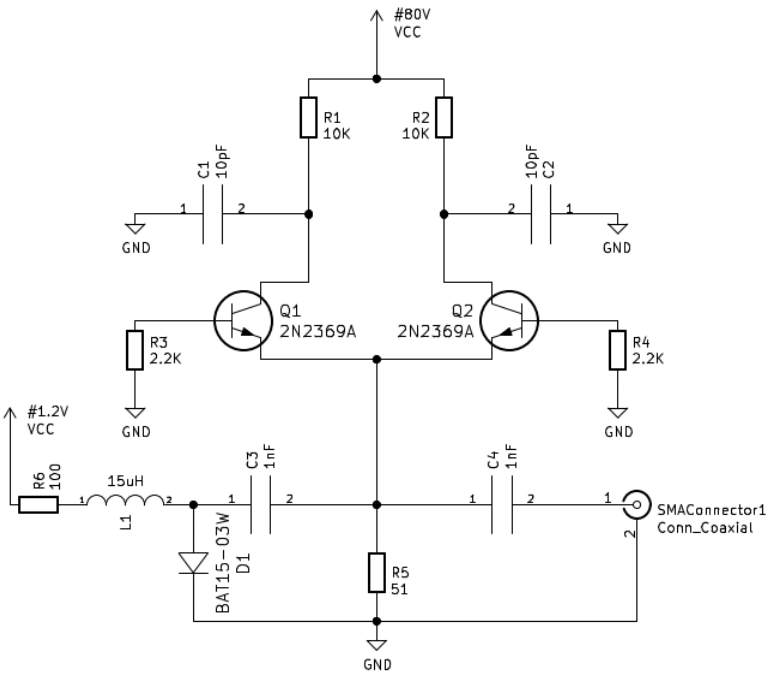

a)

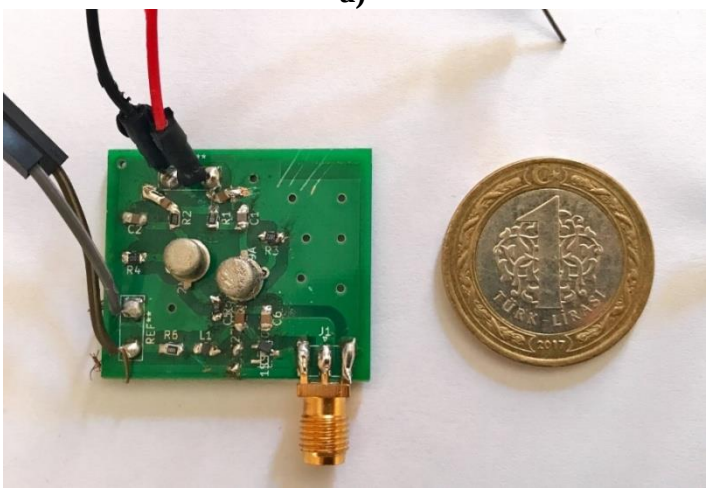

b)

Figure 3.9 (a) Schematic of the dual-transistor avalanche pulse generator with a diode mixer. (b) Photograph of the manufactured circuit.

Here, the output pulse spectrum and time domain waveform of the proposed dual-transistor pulse generator with the diode mixer circuit is given in Figure 3.10(a). As a result, the gathered values of pulse width and amplitude were 960ps and 5.28V respectively. The output pulse spectrum is depicted and compared with the 2TR – 80V result in Figure 3.10(b). As can be read, pulse spectral energy diminishes out at about 7.5 GHz completely while the 2TR – 80V circuit has still some energy at 12 GHz. From this perspective, using a mixer diode seems useless but it is supposed the reason for that is just the passive nature of the diode. The study on the V_{CC} effect which will be explained in section 3.2.3 can be proof of this hypothesis.

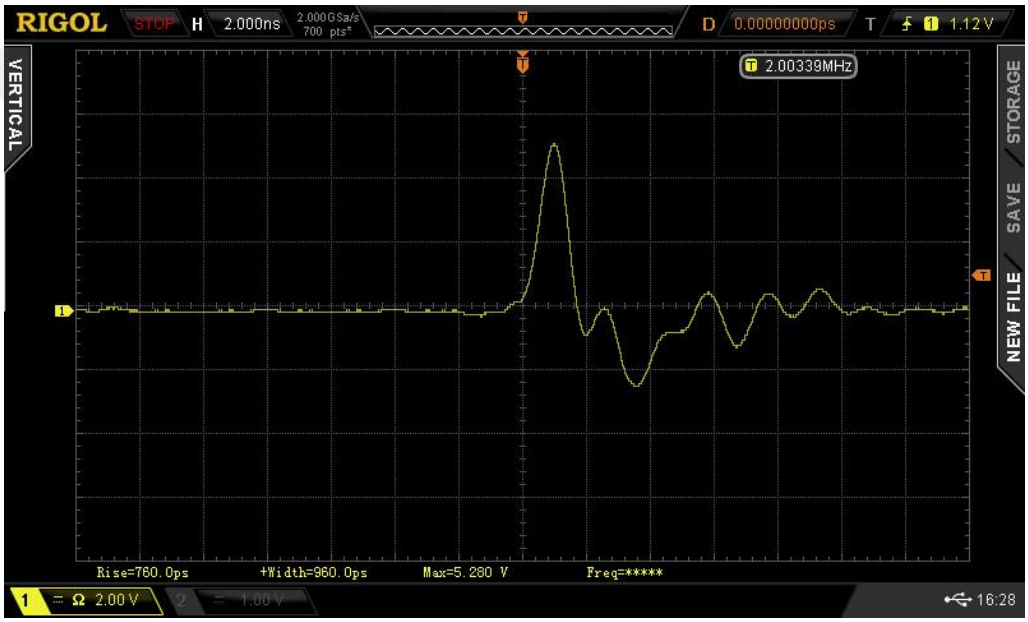

a)

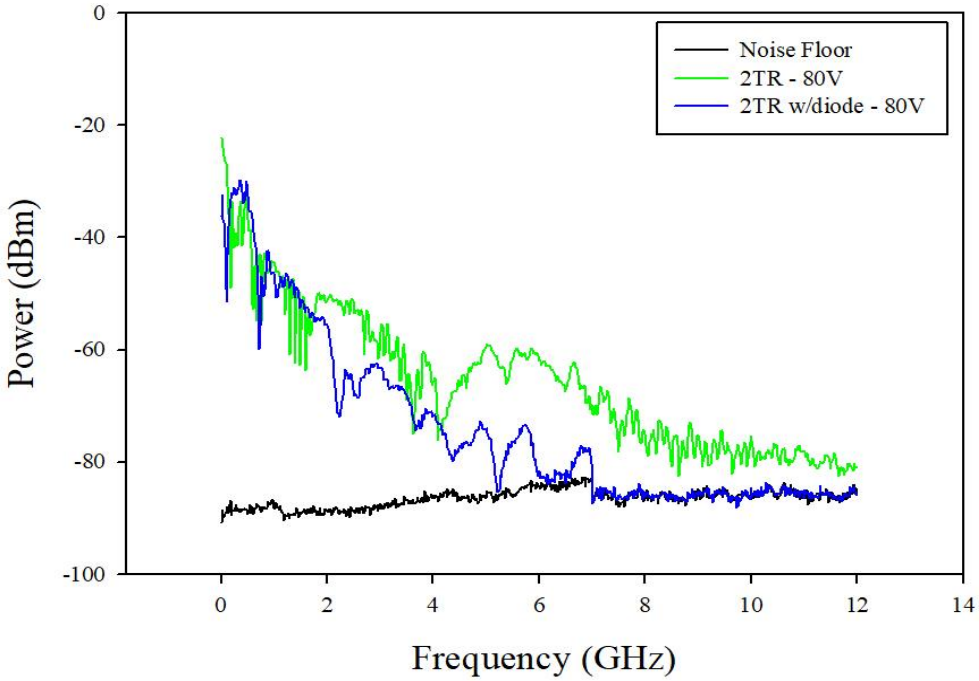

b)

Figure 3.10 (a) Output pulse in time domain, and (b) output pulse spectrum of the pulse generator with mixer diode for V_{CC}=80V.

In the following Figure 3.11, the graph compares the measured pulse spectrums for the single-transistor base circuit (1TR), dual-transistor circuit (2TR), single-transistor with diode mixer (1TR w/diode), and the dual-transistor with diode mixer (2TR w/diode).

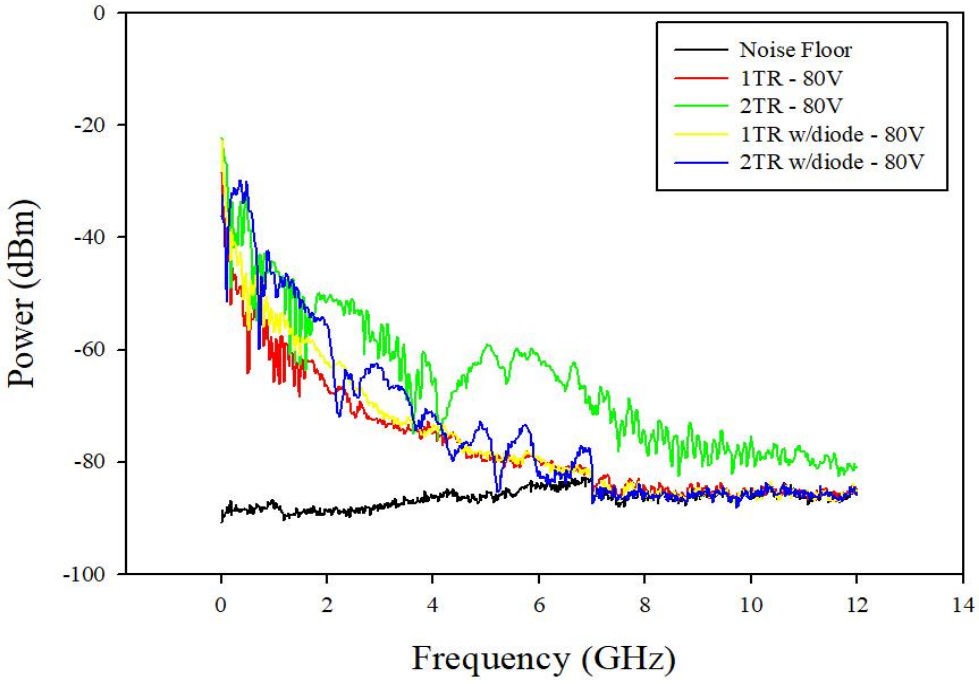

Figure 3.11 Comparison of the output spectrums of tested circuits.

The given comparison results exhibit that the dual-transistor circuit generates the highest bandwidth that can be counted as almost double the single-transistor circuit has produced and escalated output power. The mixer effect associated with Q1 and Q2 may have been the reason for this band broadening. This broadened pulse spectrum also indicates shortened pulse width. The given Figure 3.11 further proves that 1TR w/diode and 2TR w/diode circuits exhibit a slight improvement in spectral power production over single-transistor base circuits below 6 GHz. Yet, beyond 7.5 GHz, the output power shown by these circuits is at the same level as the noise floor. This may have an explanation as follows: Theoretically, there must definitely be a mixing effect due to the diode. But, the diode puts in an appearance as a parallel load next to the 50-Ω load resistor (R5) as shown in Figure 3.9(a), and the output power for the spectrum components produced by the diode's nonlinearity is significantly reduced caused by the Schottky diode mixer is inherently passive, especially above 7 GHz.

Table 3.1 Comparison of the experiment circuits.

Circuit	Pulse amplitude (V)	Pulse width (ns)
Single-transistor base circuit(1TR-80V)	7.12	1.38
Dual-transistor circuit(2TR-80V)	17.40	1.24
Single-transistor base circuit with diode mixer (1TR w/diode-80V)	5.56	1.46
Dual-transistor circuit with diode mixer(2TR w/diode-80V)	5.28	0.96

Table 3.1 reveals the values of output pulse amplitudes and pulse widths for several cases when V_{CC} arranged to 80V. Considering the results given in Table 3.1, the dual-transistor circuit shows an output pulse that has shorter pulse width and higher pulse amplitude compared to the single-transistor base circuit case. The mentioned advancement has also been certified in the frequency domain by observing the broadened bandwidth (beyond 12 GHz) and higher spectral power.

Now, two challenging question arises to be answered about measurements. Could we precisely measure an output pulse whose spectrum extends over 12 GHz while using a 300 MHz oscilloscope? And what pulse width (Gaussian waveform) has a spectrum of roughly 12 GHz? Let's start by executing a straightforward MATLAB code to address the second question. According to simulations, the needed pulse width must be less than 200ps in order to achieve a spectrum of roughly 12 GHz from a Gaussian pulse. And the oscilloscope's required bandwidth must be at least several GHz in order to accurately measure such a short pulse. Therefore, the response to the first query is No. Since we were aware of this from the outset of the thesis, we incorporated the spectrum analyzer measurements for each scenario.

3.2.3 Effect of V_{CC} on the Measured Spectrums

Another important step in the analysis was to evaluate the effect of V_{CC} by increasing it to 97V for the 2TR and 2TR w/diode circuits. Here, Figure 3.12 depicts pulse spectrum measurements. When V_{CC} is 80V, the results reveal that the 2TR circuit performs well. Because of the mixing effect produced by Q1 and Q2, it has a larger output power and a broader pulse spectrum. When V_{CC} rises to 97V, the output power

of the 2TR w/diode circuit rises as well, and its performance approaches that of the 2TR circuit for V_{CC}=80V. This could be owing to the faster charging of capacitors C1 and C2 in Figure 3.9(a), which hold the charge for the avalanche effect, so that may boost output power. Overall, the 2TR circuit works better than the 2TR w/diode since it is more straightforward and has a lower V_{CC} of 80V. Pulse amplitude and width measurements for the 2TR with diode circuit for V_{CC}=97V are 1.04ns and 4.8V, respectively. For the 2TR circuit with V_{CC}=97V, these readings were 1.30ns and 9.2V.

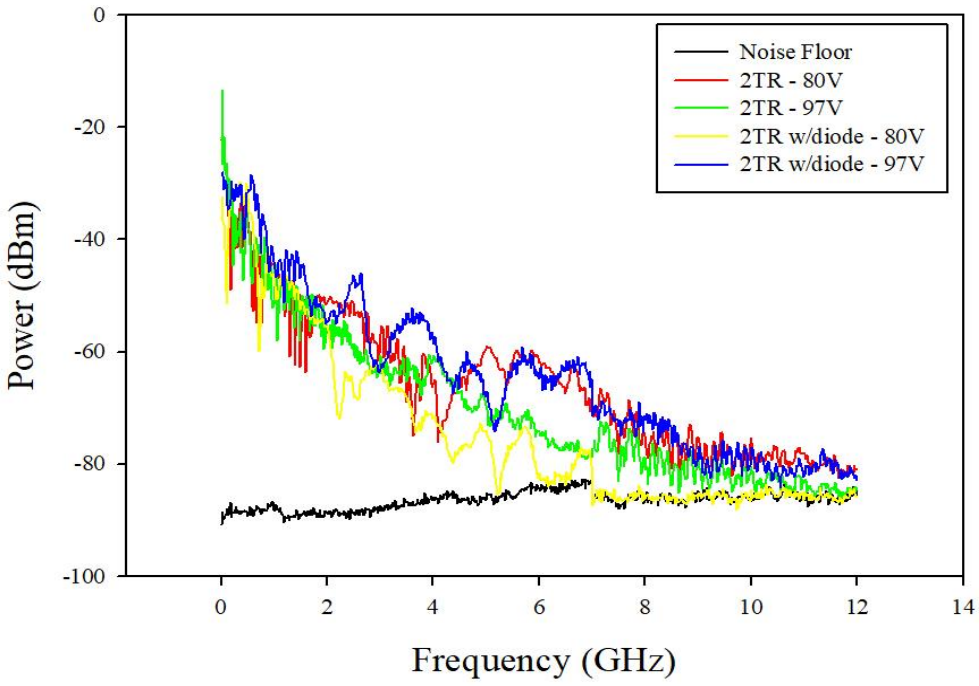

Figure 3.12 Comparison of the output spectrums of dual-transistor circuits for different V_{CC} values.

In order to conduct further research, Table 3.2 compares the performance of the dual-transistor circuit described in this thesis with that of (Omurzakov et al., 2016). The given circuit design with this thesis offers a positive pulse, a narrower pulse width, a unique design, and a lower supply voltage than (Omurzakov et al., 2016).

Table 3.2 Comparison of this work and a reference.

Circuit	This work	Ref. (Omurzakov et al. 2016)
V_{CC} (V)	80	375
Pulse width (ns)	1.24	1.5
Pulse amplitude (V)	17.40@10pF discharge capacitor	140V@10pF discharge capacitor
Number of active elements in avalanche section	2	2
Requires a separate triggering circuit?	No	Yes
Pulse spectrum presented?	Yes	No
Pulse polarity	Positive	Negative

Many UWB devices, including wall imaging systems, GPRs, medical systems, and communications systems, operate in the 3.1–10.6 GHz frequency range. The given circuit conforms with the 3.1–10.6 GHz band's FCC spectral mask as can be seen in Figure 3.13. Yet, below 3.1 GHz, the given design is not conformed by the spectral mask. To satisfy the FCC specifications below 3.1 GHz, a straightforward high-pass filter may be employed after the pulse generator. Therefore, a few slight circuit-level optimizations or adjustments are needed for UWB systems. By modulating the produced pulse suitably, the suggested circuit may be employed in UWB systems. OOK-type modulation is readily accomplished by correctly high-pass filtering the resulting Gaussian pulse and turning the pulses ON and OFF with the binary input data once the FCC mask is fulfilled. Other modulation techniques, such as PPM and PAM, need more intricate circuitry.

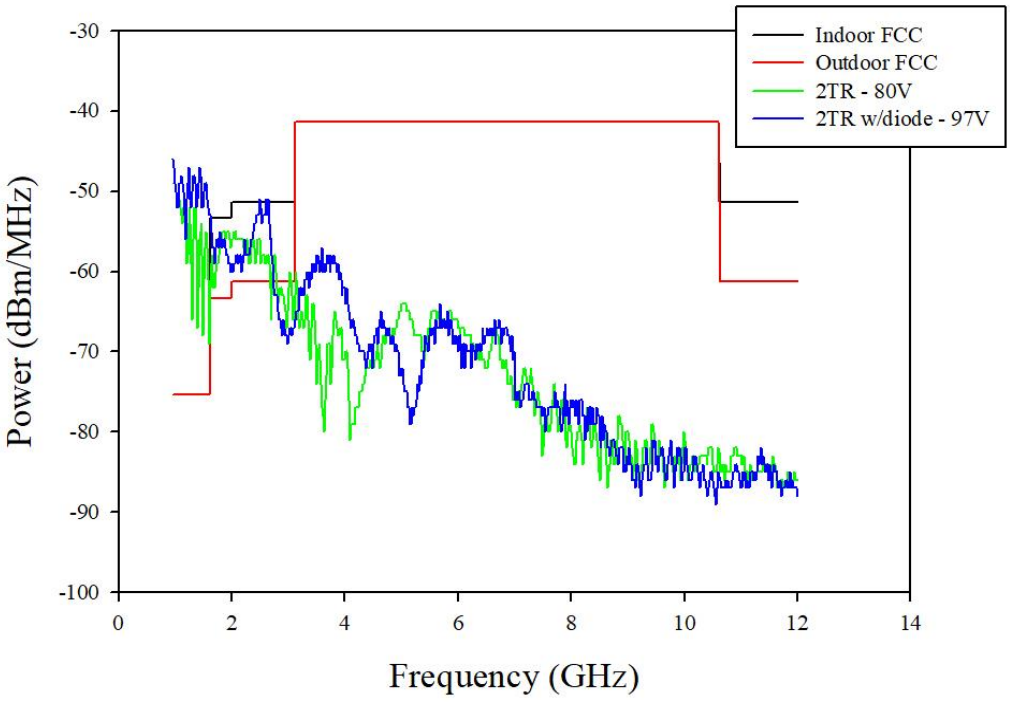

Figure 3.13 Spectral mask and the spectrums of proposed circuit designs.

3.3 Avalanche Pulse Generator with Control Over Pulse Amplitude and Pulse Width

The avalanche pulse generator circuit described in previous chapters is self-triggered and appears to have no control over pulse amplitude and pulse width. Two different techniques are presented in this section. In section 3.3.1, the simple single transistor avalanche pulse generator circuit was modified to inject a trigger signal to the base terminal through a coupling capacitor. The injected signal is a 1V amplitude square wave with 50% duty cycle and its frequency is varied to examine any changes in the output pulse amplitude. In section 3.3.2 a different technique, involving a varactor diode, was implemented to control both the pulse width and pulse amplitude.

3.3.1 Single Transistor Circuit with External Trigger Signal

The circuit with external trigger input is shown in Figure 3.14(a). The base terminal is injected by a 1V amplitude square wave supplied by a function generator. Frequency of the square wave was varied to observe amplitude changes of the output pulse. V_{CC} was set to 80V and the component values are the same as those in the base circuit. The schematic is the same except the base circuitry part and the circuit board was changed slightly to accommodate trigger signal input to the base terminal. The schematic and the PCB are shown in Figure 3.14(a) and (b), respectively.

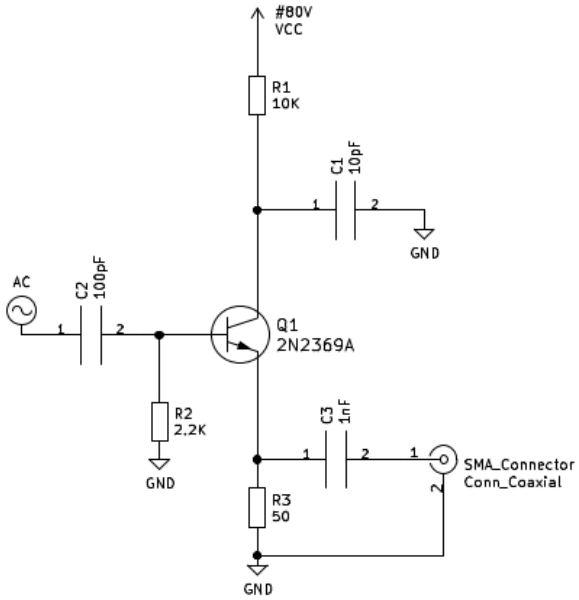

(a)

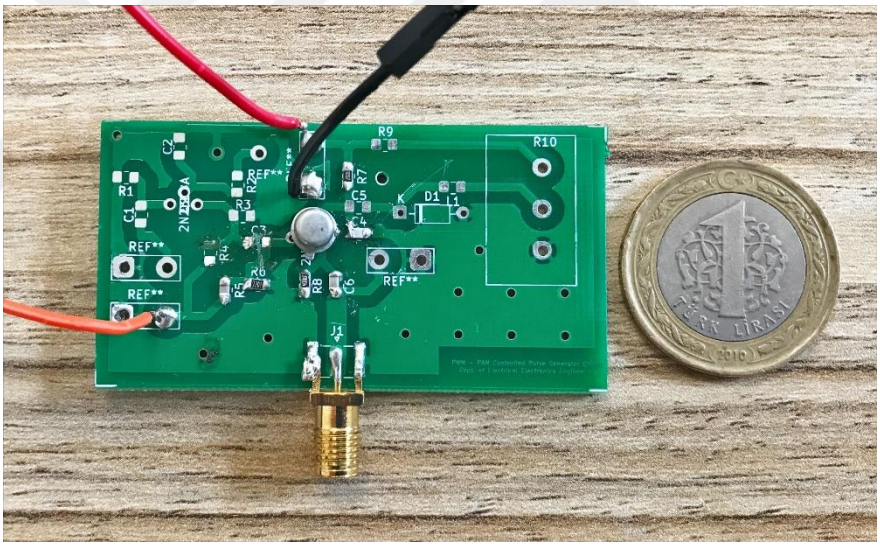

(b)

Figure 3.14 (a) Modified single-transistor avalanche pulse generator schematic, (b) manufactured circuit.

Figure 3.15 shows the time-domain output pulse of the circuit in Figure 3.14(a) without any trigger signal at the base terminal. For this case, pulse amplitude and pulse width are measured as 10V and 1.38ns, respectively. Pulse repetition frequency is about 111 kHz. To investigate the effect of external trigger signal over the pulse amplitude, a 1V amplitude square wave with 50% duty cycle was injected to the base terminal of Q1 at

200 kHz, 2 MHz, 2.5 MHz, 3 MHz, and 10 MHz. The results are shown in Figures 5.3-5.7 and summarized in Table 3.3.

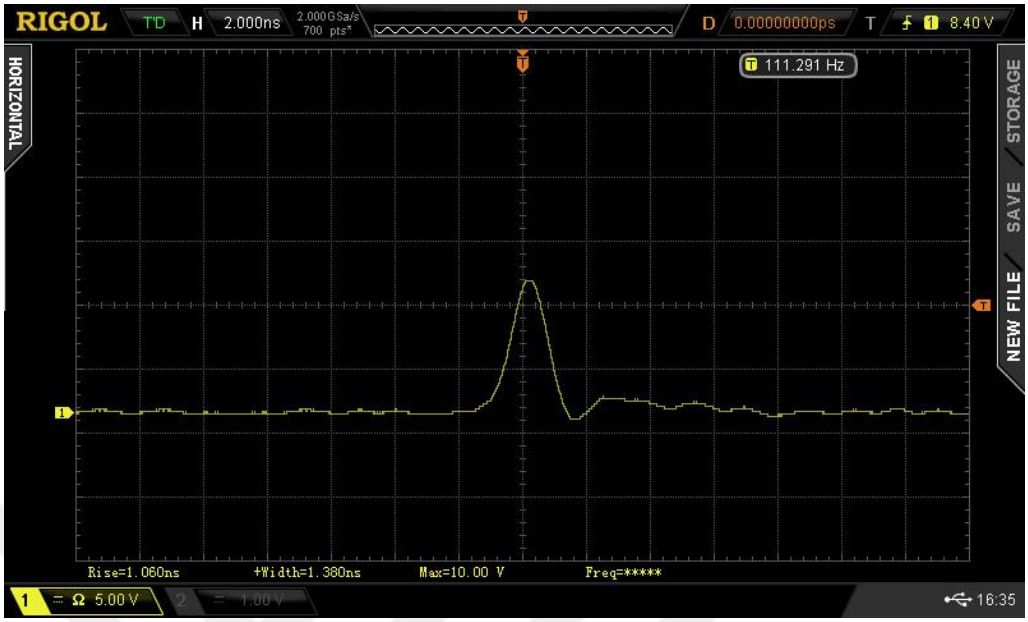

Figure 3.15 Output pulse without trigger signal injected at the base terminal.

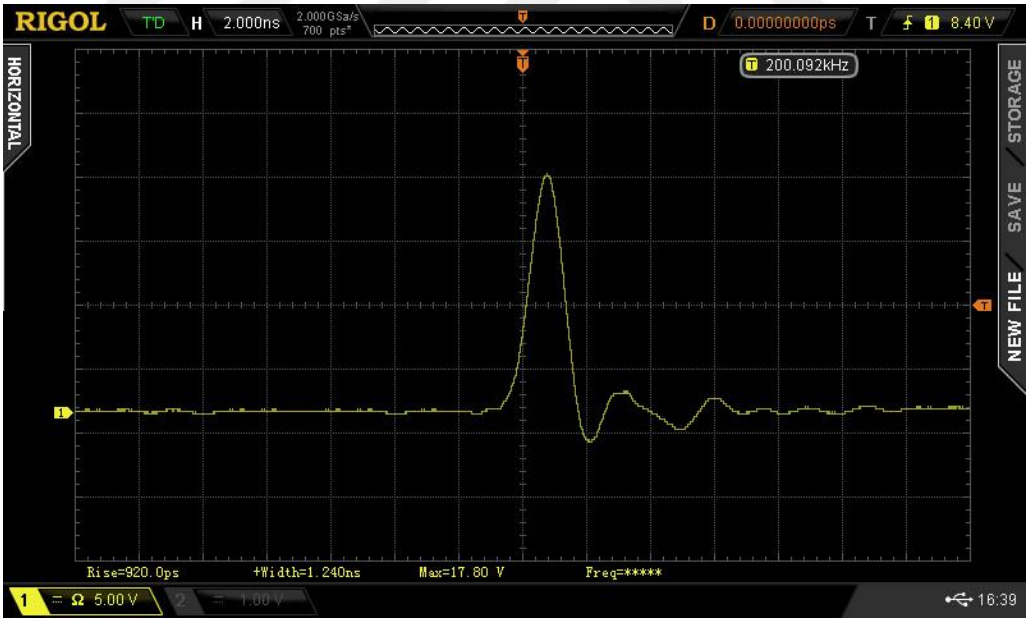

Figure 3.16 Output pulse with 200 kHz – 1V trigger signal at the base terminal.

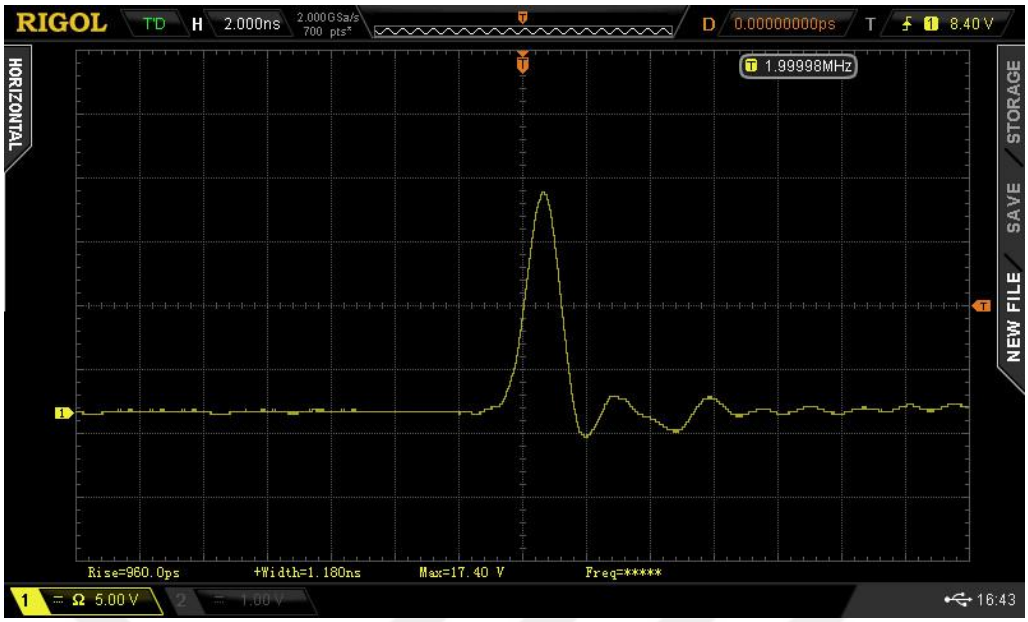

Figure 3.17 Output pulse with 2 MHz – 1V trigger signal at the base terminal.

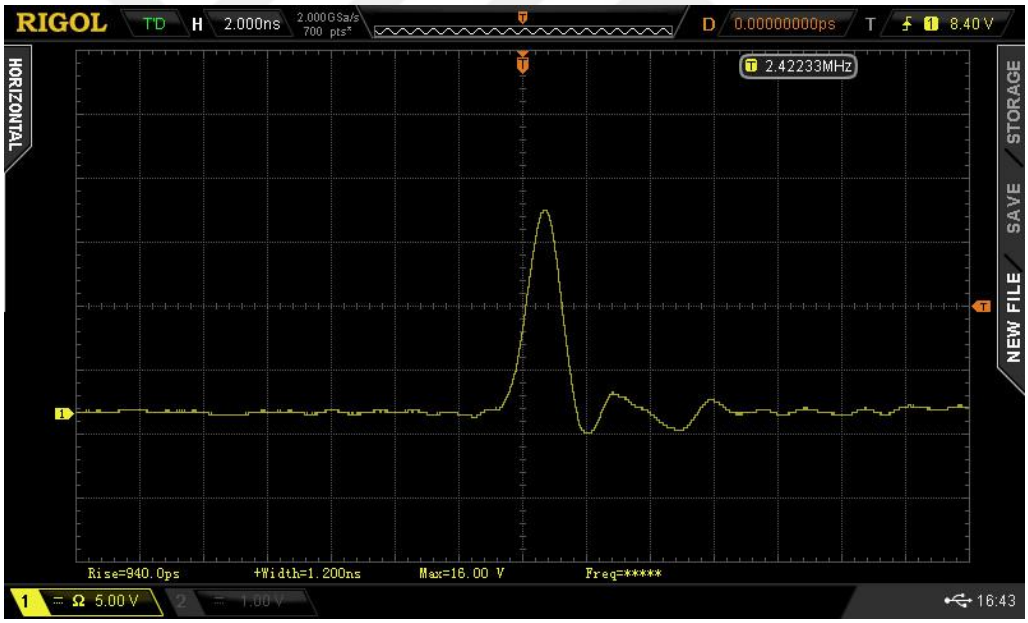

Figure 3.18 Output pulse with 2.5 MHz – 1V trigger signal at the base terminal.

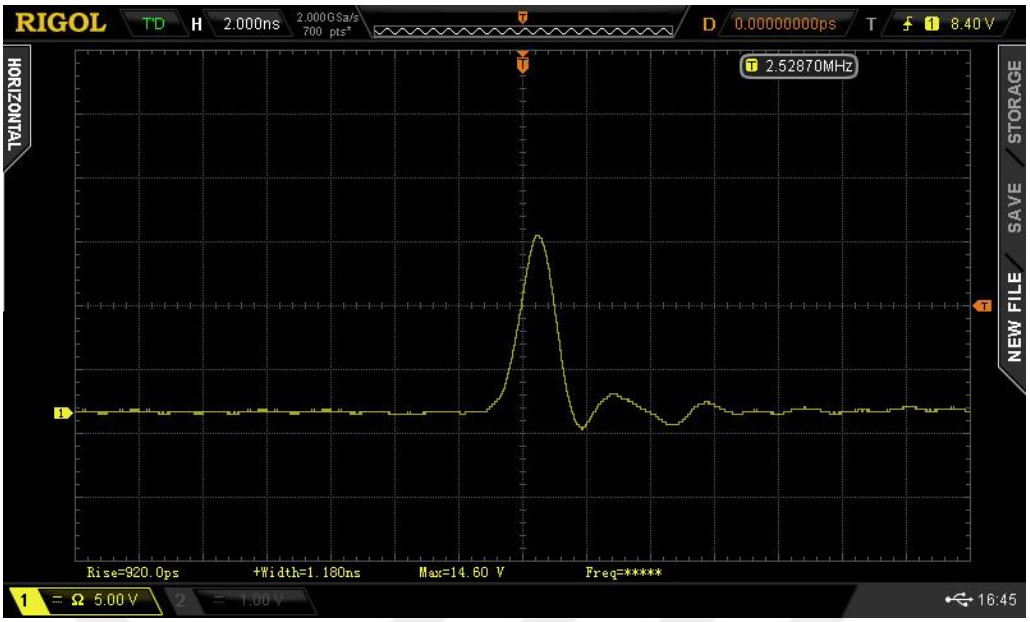

Figure 3.19 Output pulse with 3 MHz – 1V trigger signal at the base terminal.

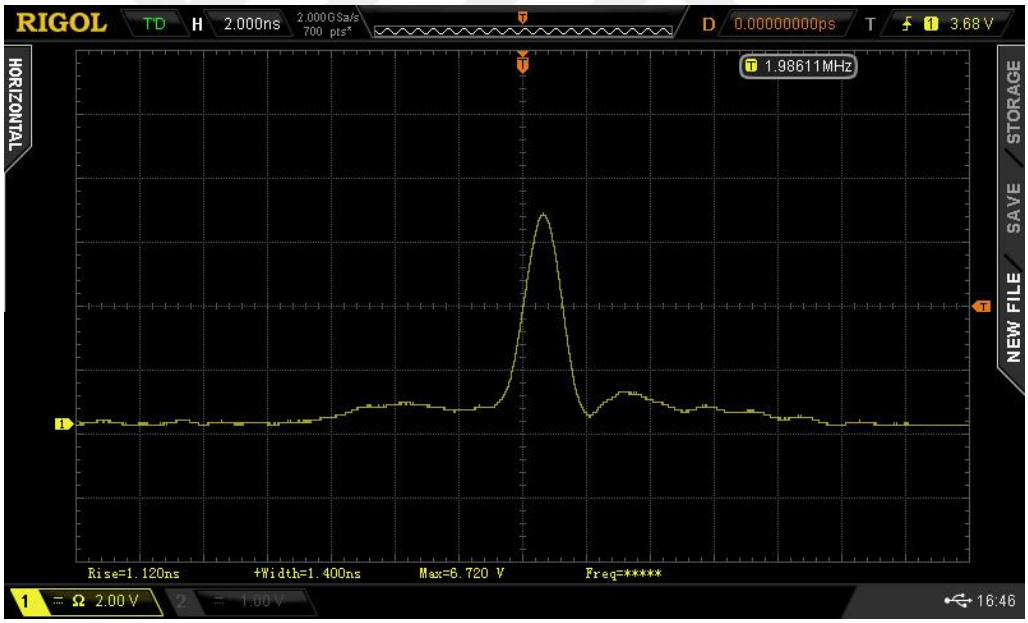

Figure 3.20 Output pulse with 10 MHz – 1V trigger signal at the base terminal.

Compared to the “no signal at base” reference case, applying a 200 kHz 1V square wave to the base terminal results in an increase for the pulse amplitude and decrease for the pulse width. New pulse amplitude is 17.8V which is a substantial improvement over the 10V amplitude of the reference case. The reason for this improvement can be explained as follows. When the transistor avalanches, C1 is discharged onto R3. If

there is no external trigger signal, avalanche takes place at the natural resonant frequency of the circuit which is the charge-discharge cycle of C1 set by avalanche phenomenon. However, in the presence of an external trigger signal, the transistor also provides current gain due to amplification of the base current, and this in turn results in higher collector current in addition to the collector current due to avalanche effect. And the result is further increase of the output pulse amplitude. When the input signal is 200 kHz and 2 MHz 1V square waves, pulse amplitude is maximum at about 17.6V whereas the pulse width is about 1.2 ns. Further increase of the frequency of the injected signal still provides high amplitude pulses up to few MHz. However, pulse amplitude drops below that of the reference case for the 10 MHz trigger signal.

Another observation is the pulse repetition frequency, PRF. Table 3.3 shows that when the input frequency is equal to the PRF, output pulse has the highest amplitude. This is indeed the case for 200 kHz and 2 MHz input signals which result in 200 kHz and 2 MHz PRFs, respectively. When the measured PRF is lower than the frequency of the trigger signal, maximum pulse amplitude can not be achieved. PRF can be controlled by an external base signal, and so the discharge frequency of the charged capacitor is controlled. At lower trigger frequencies, the circuit has enough time to charge the capacitor fully and so the PRF is equal to the frequency of the trigger signal. When the trigger signal frequency is high, the circuit can not fully charge the capacitor so the pulse amplitude gets lower.

Table 3.3 Comparison of output pulse properties when the base terminal is driven by a square wave at different frequencies.

Frequency of the injected signal	Pulse amplitude (V)	Pulse width (ns)	PRF (kHz)
No signal at base	10.00	1.38	111
200 kHz	17.80	1.24	200
2 MHz	17.40	1.18	2000
2.5 MHz	16.00	1.20	2422
3 MHz	14.60	1.18	2528
10 MHz	6.72	1.40	1986

3.3.2 Single-Transistor Circuit with Varactor Diode

In this part of the study, the single-transistor base circuit is modified by adding a varactor diode to control the pulse width at the output. Since the pulse width is dependent on the collector capacitance, a suitable modification was done around the collector capacitance C1 (10pF) as shown in Figure 3.21(a). The selected varactor diode is BB809 (D1) due to availability of the part. BB809 shows a minimum capacitance of about 5pF under 28V reverse bias and a maximum capacitance of about 46pF under 1V reverse bias according to the datasheet (Anon 1996). C1 and the capacitance of D1 are connected in parallel as shown in Figure 3.21(a). Manufactured circuit is shown in Figure 3.21(b). Let's denote the capacitance of D1 as Cd(*V*). Since the minimum and maximum capacitances of the varactor diode are 5pF and 46pF, respectively, the equivalentcollector capacitance ranges from C1+Cd(28V)=10pF+5pF=15pF to C1+Cd(1V)=10pF+46pF=56pF.

D1 is reverse biased through a voltage divider network composed of R4 and R5 and an RF choke L1 (15μH). C4 is a 10nF dc block capacitor. It has minimal effect over the equivalent collector capacitance formed by C1 and D1. The presented circuit also has external trigger signal input which is connected to the base terminal of Q1 through C2.

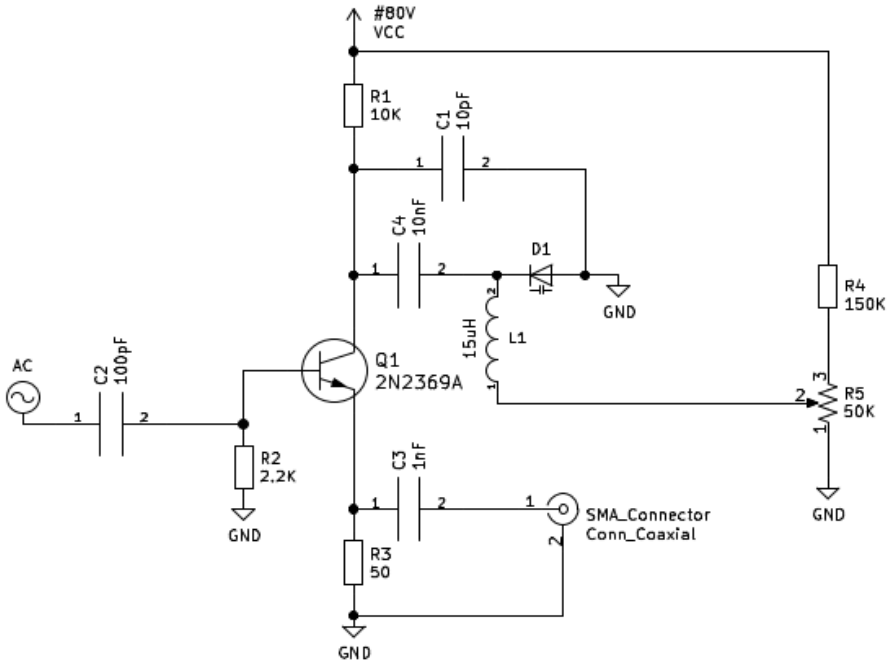

(a)

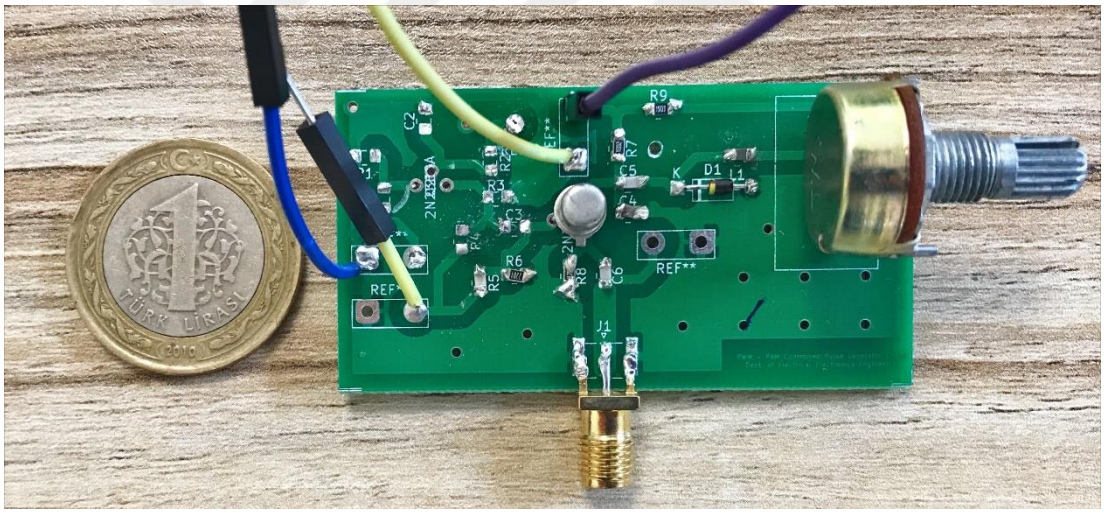

(b)

Figure 3.21 (a) Single-transistor circuit with varactor diode. (b) Manufactured circuit.

Figure 3.22 shows the output pulse of the modified circuit with a varactor diode. A 1.5 MHz square wave with 50% duty cycle and 1V amplitude was injected to the base. And the reverse bias on D1 is 1V so Cd(1V)=46pF. As a result, the equivalent collector capacitance Cec is 56 pF for the result shown in Figure 3.22. Pulse shape is distorted as can be seen, and this may be due to the varactor diode selection since it is actually a VHF varactor diode.

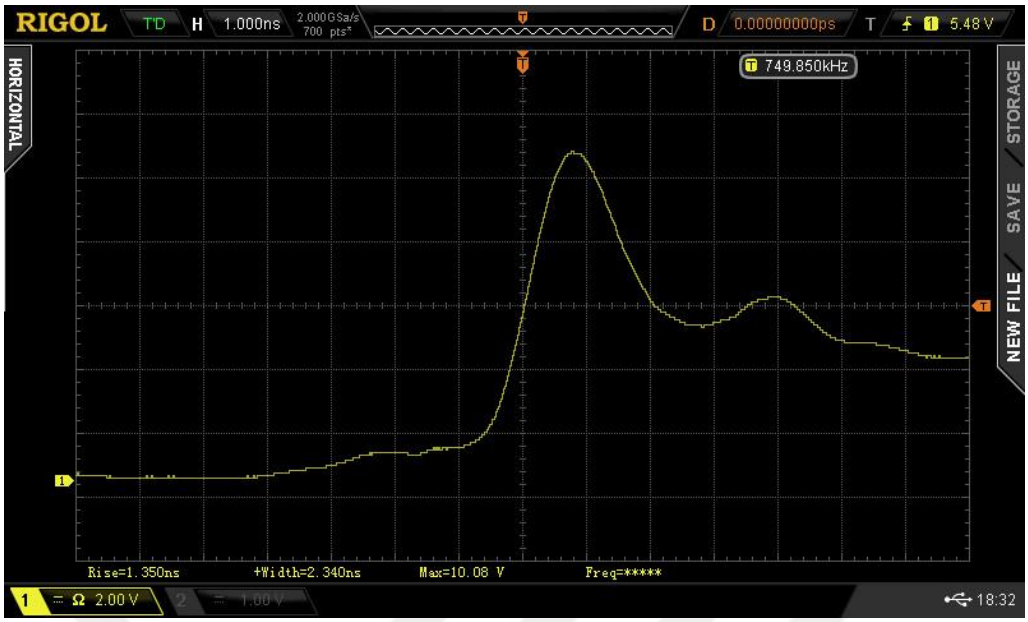

Figure 3.22 Output pulse when the injected signal is 1.5 MHz square wave with 1V amplitude. Cd=46pF and Cec=56pF.

Figure 3.23 shows the output pulse of the modified circuit with a varactor diode when the reverse bias is 28V. A 1.5 MHz square wave with 50% duty cycle and 1V amplitude was injected to the base. Since Cd(28V)=5pF, the equivalent collector capacitance Cec is 15 pF for this case.

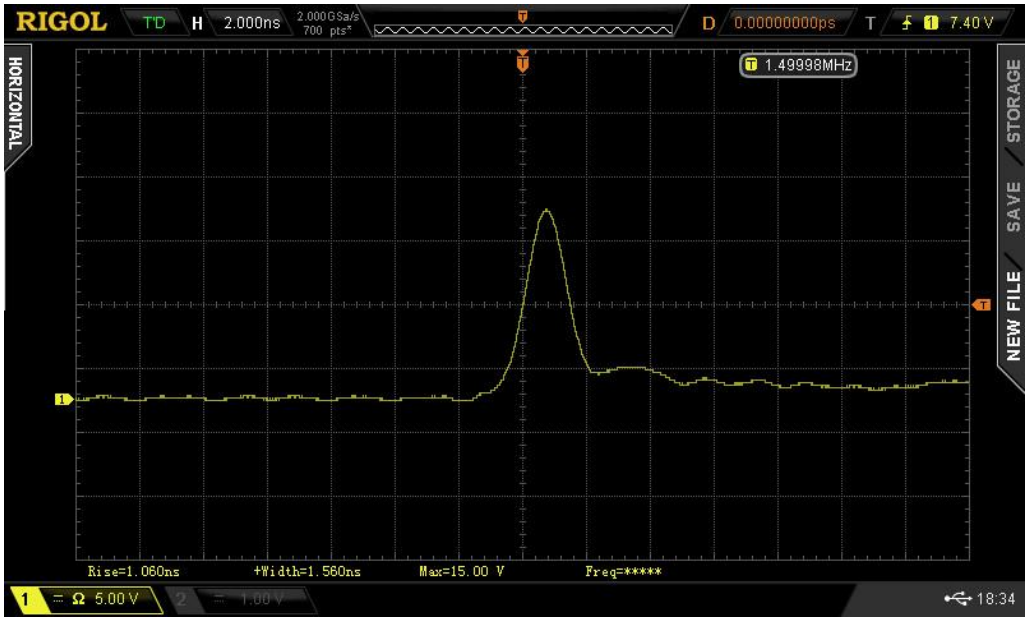

Figure 3.23 Output pulse when the injected signal is 1.5 MHz square wave with 1V amplitude. Cd=5pF and Cec=15pF.

Results of Figure 3.22 and Figure 3.23 are summarized in Table 3.4 with a trigger signal of 1.5 MHz and 1V amplitude. When Cd=5pF the PRF is 1.5 MHz indicating the equivalent collector capacitance is fully charged and discharged at the rate of the trigger signal. When Cd=46pF, a higher amplitude is expected. However, since PRF is 750 kHz now, Cec can not be charged fully. Therefore, the output pulse amplitude is lower than that of the Cd=5pF case. On the other hand, Table 3.4 also shows that pulse width can be varied from about 1.5ns to 2.3ns by varying the voltage of the varactor diode.

Table 3.4 Comparison of output pulse properties with varying capacitance values with a trigger signal of 1.5 MHz at 1V amplitude.

Cd (pF)	Cec (pF)	Pulse amplitude (V)	Pulse width (ns)	PRF (kHz)
5	15	15.00	1.56	1500
46	56	10.08	2.34	750

By using the same circuit structure, to see the pulse amplitude changes, different frequencies were injected into the base terminal of the transistor. For this case, capacitance Cd of the varactor diode is about 20pF and this makes the Cec as 30pF. The capacitance values of varactor diode were approximated by checking the I_C versus Cd curve value from a graph at the applied reverse biased voltage (Anon 1996). In Figure 3.24 and Figure 3.25, results for 200 kHz and 500 kHz – 1V injected signal cases are given. And results continue with increasing triggering signal frequencies from Figure 3.26 to Figure 3.30, and they are summarized in Table 3.5.

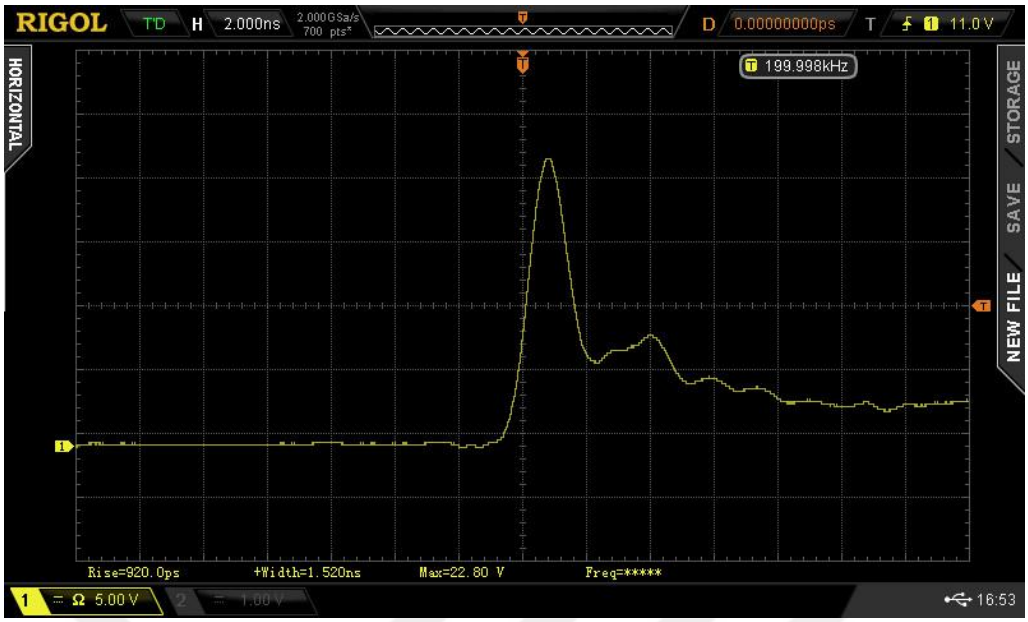

Figure 3.24 Output pulse with 200 kHz – 1V injected signal when Cd=20pF and Cec=30pF.

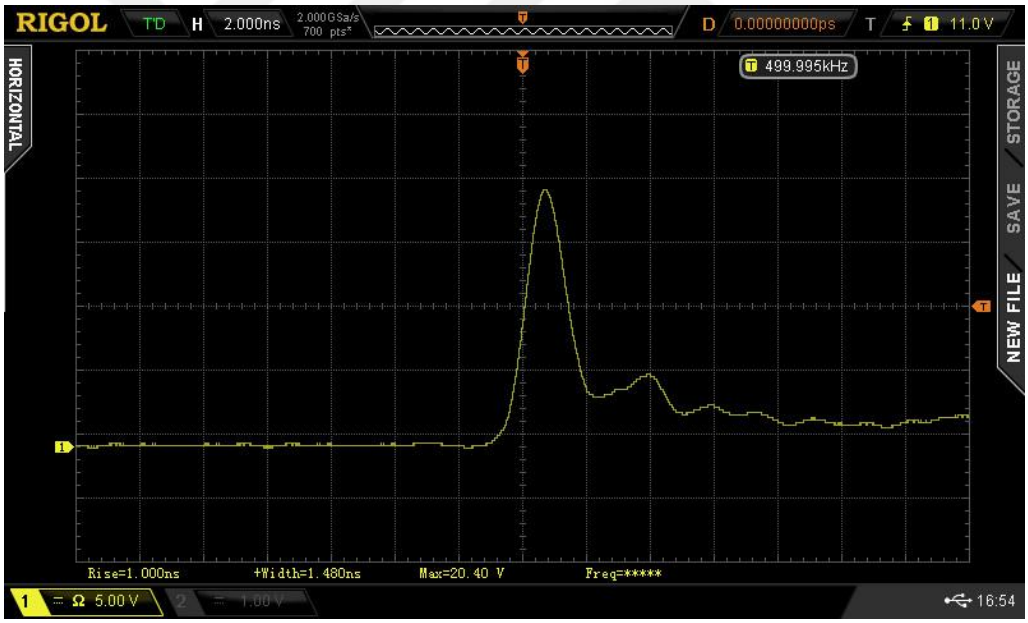

Figure 3.25 Output pulse with 500 kHz – 1V injected signal when Cd=20pF and Cec=30pF.

In Figure 3.26 result for 1 MHz – 1V injected signal is given for Cd=20pF and Cec=30pF.

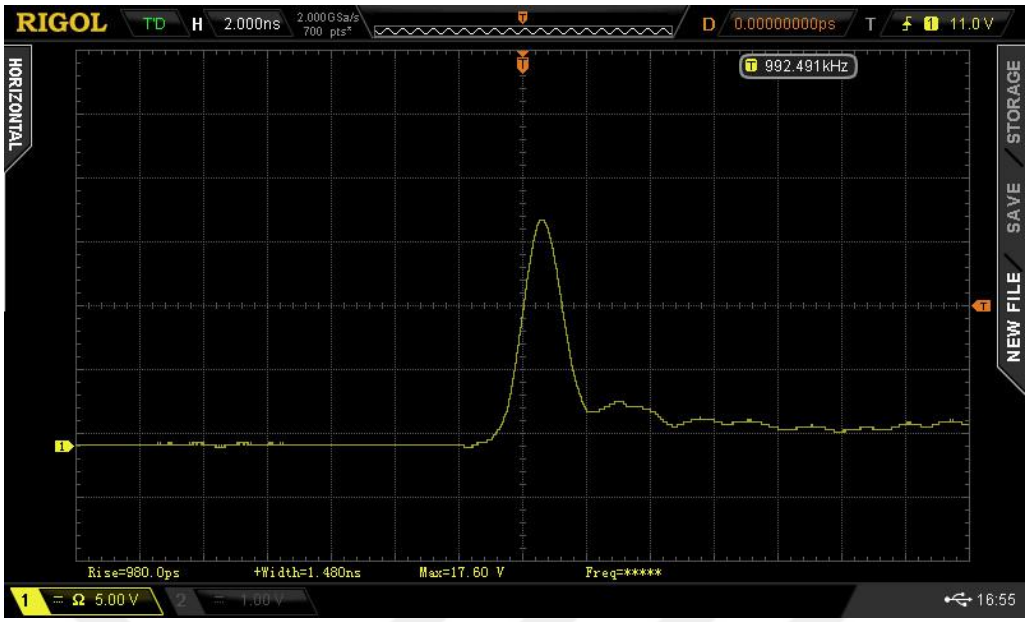

Figure 3.26 Output pulse with 1 MHz – 1V injected signal when Cd=20pF and Cec=30pF.

In Figure 3.27 result with 1.5 MHz – 1V injected signal is given for Cd=20pF and Cec=30pF.

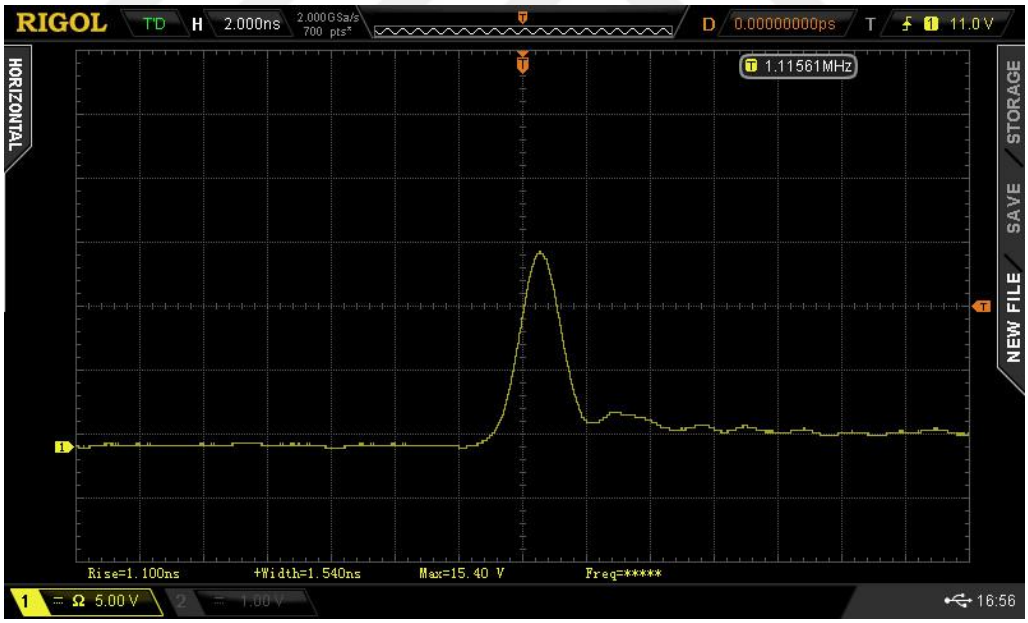

Figure 3.27 Output pulse with 1.5 MHz – 1V injected signal when Cd=20pF and Cec=30pF.

In Figure 3.28 result with 2 MHz – 1V injected signal is given for Cd=20pF and Cec=30pF.

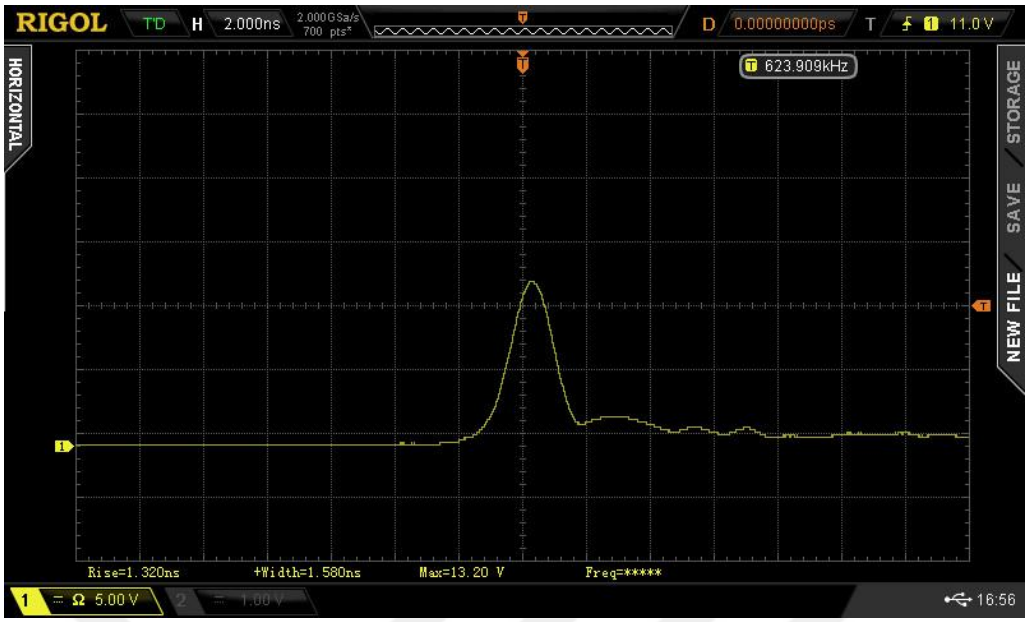

Figure 3.28 Output pulse with 2 MHz – 1V injected signal when Cd=20pF and Cec=30pF.

In Figure 3.29 result with 3 MHz – 1V injected signal is given for Cd=20pF and Cec=30pF.

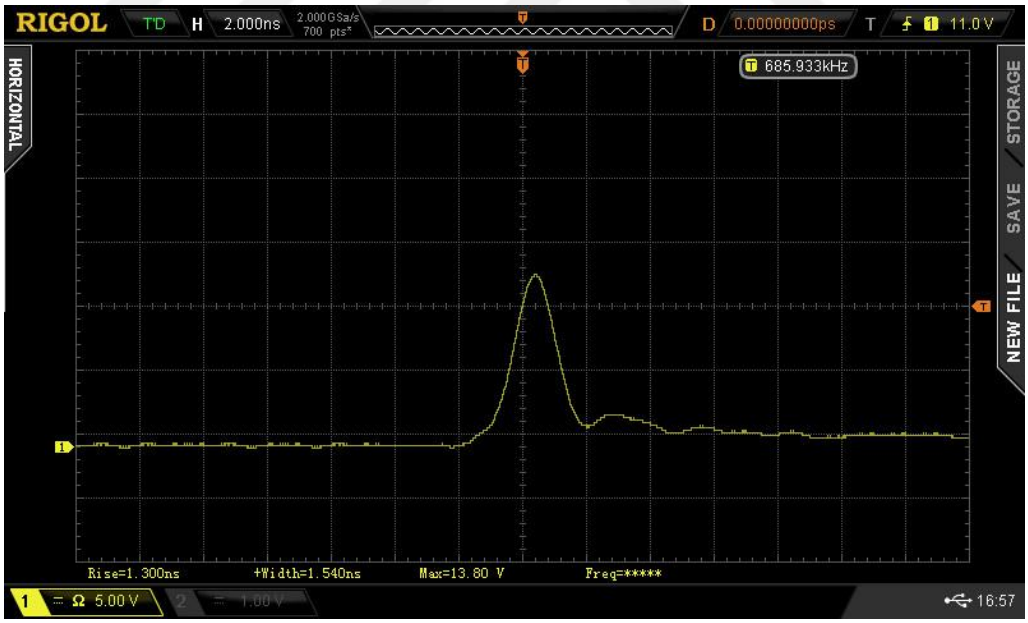

Figure 3.29 Output pulse with 3 MHz – 1V injected signal when Cd=20pF and Cec=30pF.

In Figure 3.30 result with 5 MHz – 1V injected signal is given for Cd=20pF and Cec=30pF and all above given results are summarized in Table 3.5.

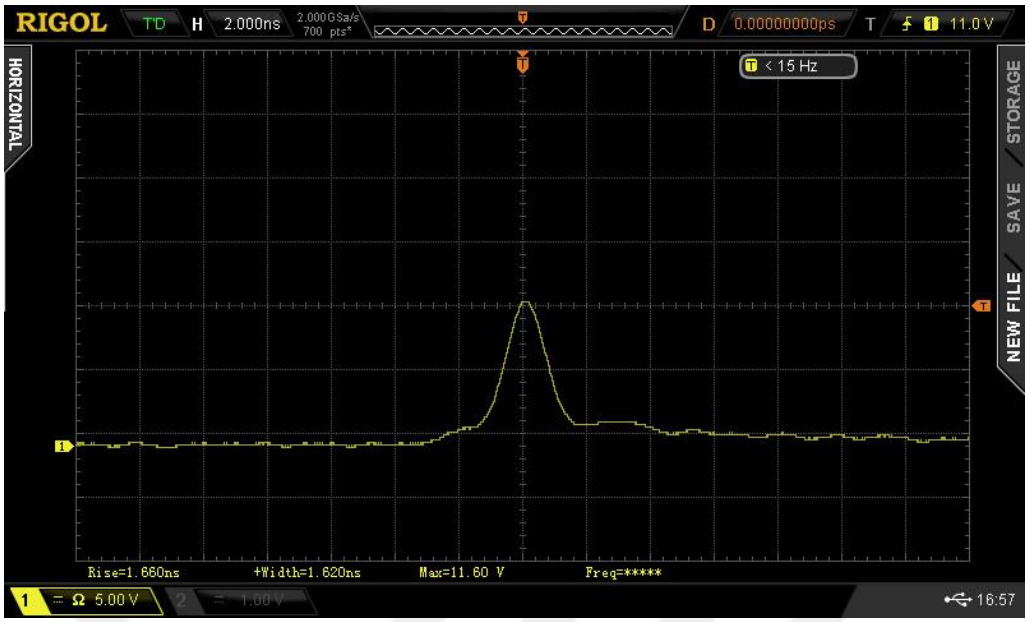

Figure 3.30 Output pulse with 5 MHz – 1V injected signal when Cd=20pF and Cec=30pF.

Table 3.5 Comparison of pulse properties with varying frequencies of the trigger signal for a fixed Cec value of 30pF.

Frequency of the trigger signal	Cd (pF)	Cec (pF)	Pulse amplitude (V)	Pulse width (ns)	PRF (kHz)
200 kHz	20	30	22.80	1.52	200
500 kHz	20	30	20.40	1.48	500
1 MHz	20	30	17.60	1.48	992
1.5 MHz	20	30	15.40	1.54	1115
2 MHz	20	30	13.20	1.58	623.9
3 MHz	20	30	13.80	1.54	685.9
5 MHz	20	30	11.60	1.62	<15Hz

Here PRF helps us to understand confusing amplitude values. The base circuit is able to catch up the triggering signal's frequency up to almost 2.5 MHz, but in here, with the inclusion of the varactor diode circuitry, 1 MHz is the top frequency value that the circuit giving the best response in terms of amplitude. Thus, while 2 MHz and 200 kHz amplitude values gave the best results in the base circuit, here, 200 kHz and 500 kHz gave the best amplitude results. Basically, the base circuit have 10pF capacitance and

it is quicker to fill it. Now the capacitance is 30pF and 1 MHz trigger signal can barely fill it.

4. CONCLUSIONS

It is constructed and presented a novel, simple, and low-cost dual-transistor pulse generator circuit employing self-triggered BJTs in avalanche mode with mixing effect. In comparison to the reference single-transistor design, the suggested circuit delivers greater output power without the need of a power amplifier and provides a shorter pulse width and a broader spectral energy. Furthermore, when compared to other reference studies, it has better output pulse qualities such as stability, positive pulse, and so on. In this thesis, the same mixing effect is investigated using a passive Schottky diode, and promising findings are obtained. This thesis also includes pulse amplitude and pulse width control studies over the base circuit to meet the demands of many different areas. All of these features make the proposed circuit suitable for ground-penetrating radar, remote sensing, and ultra-wideband communications.

REFERENCES

Ahajjam, Younes, Otman Aghzout, Josè M. Catala-Civera, Felipe Peñaranda-Foix, and Abdellah Driouach. 2020. "Two-Stage Design of High Power UWB Monocycle Generator for Radar Sensor Applied in the Fourth Industry Revolution." *Procedia Manufacturing* 46:730–37.

Ameri, Ahmed Abbas H., Günter Kompa, and Axel Bangert. 2011. "Balanced Pulse Generator for UWB Radar Application." Pp. 198–201 in *2011 8th European Radar Conference*.

Anon. 1996. "Discrete Semiconductors, BB809 VHF Variable Capacitance Diode, Philips." 4. Retrieved (https://www.alldatasheet.com/datasheet-pdf/pdf/16078/PHILIPS/BB809.html).

Anon. 2004. "PN2222A, NPN General-Purpose Amplifier." Retrieved (https://www.mouser.com/datasheet/2/149/PN2222A-889968.pdf).

Anon. 2014. "2N2369A, Silicon NPN Transistor, Central Semiconductor Corp."

Anon. 2018. "BAT15-03W, Single Silicon RF Schottky Diode, Infineon." Retrieved (https://www.infineon.com/cms/en/product/rf/rf-diode/rf-mixer-and-detector-schottky-diode/bat15-03w/?redirId=192647).

Anon. 2021. "IRF840 Power MOSFET, Vishay Siliconix."

Anon. 2022a. "555 Precision Timers, Texas Instruments." Retrieved (https://www.ti.com/lit/ds/symlink/ne555.pdf).

Anon. 2022b. "Industry-Standard Dual Operational Amplifiers, Texas Instruments." Retrieved (https://www.ti.com/product/LM358/part-details/LM358P).

Anon. 2022c. "Oscilloscope History and Milestones, OScopes." Retrieved (http://www.oscopes.info/background/2265-oscilloscope-milestones).

Arafat, M. A., and A. B. M. Harun-ur-Rashid. 2012. "A Novel 7 Gbps Low-Power CMOS Ultra-Wideband Pulse Generator." *IET Circuits, Devices \& Systems* 6(6):406–12.

Bennett, C. Leonard, and Gerald F. Ross. 1978. "Time-Domain Electromagnetics and Its Applications." *Proceedings of the IEEE* 66(3):299–318.

Bracewell, Ronald Newbold, and Ronald N Bracewell. 1986. *The Fourier Transform and Its Applications*. Vol. 31999. McGraw-Hill New York.

Chadderton, Neil. 1996. "The ZTX415 Avalanche Mode Transistor." *Zetex Application Note*.

Chang, Kai, Vijay Nair, and Inder J. Bahl. 2001. *RF and Microwave Circuit and Component Design for Wireless Systems*. John Wiley \& Sons, Inc.

Davis, W. Alan, and Krishna Agarwal. 2003. *Radio Frequency Circuit Design*. John Wiley \& Sons.

Dias, José A. Siqueira. 2005. "On the Avalanche Multiplication Mechanism in SPICE Simulations of High-Frequency Bipolar Transistors with Thin Basewidths and Low Breakdown Voltages." *AEU-International Journal of Electronics and Communications* 59(8):483–85.

Federal Communications Commission. 2002. “Revision of Part 15 of the Commission’s Rules Regarding Ultra-Wideband Transmission Systems.” *First Report and Order* FCC--02.

Fontana, Robert J. 2002. “Recent Applications of Ultra Wideband Radar and Communications Systems.” Pp. 225–34 in *Ultra-Wideband, Short-Pulse Electromagnetics 5*. Springer.

Guo, Y., and G. Zhu. 2014. “Novel Design and Implementation of Ultra-Wideband Pulse Generator Based on Avalanche Transistor.” *Progress in Electromagnetics Research Symposium* (January 2014):34–38.

Horowitz, Paul, Winfield Hill, and Ian Robinson. 1989. *The Art of Electronics*. Vol. 2. Cambridge university press Cambridge.

Jaeger, Richard C., and Travis N. Blalock. 1997. *Microelectronic Circuit Design*. McGraw-Hill New York.

Kamegai, Naoki, Shigeru Kishimoto, Koichi Maezawa, Takashi Mizutani, Hiroya Andoh, Kazuhiro Akamatsu, and Hirofumi Nakata. 2008. “Ultrashort Pulse Generators Using Resonant Tunneling Diodes and Their Integration with Antennas on Ceramic Substrates.” *Japanese Journal of Applied Physics* 47(4S):2833.

Matiss, A., A. Poloczek, A. Stohr, W. Brockerhoff, W. Prost, and F. J. Tegude. 2007. “Sub-Nanosecond Pulse Generation Using Resonant Tunneling Diodes for Impulse Radio.” Pp. 354–59 in *2007 IEEE International Conference on Ultra-Wideband*.

Miller, Edmund K. 1986. *Time-Domain Measurements in Electromagnetics*. Springer Science \& Business Media.

Morgan, A. M. 1994. “Ultra-Wideband Impulse Scattering Measurements.” *IEEE Transactions on Antennas and Propagation* 42(6):840–46.

Omurzakov, Aitykul, Ahmet K. Keskin, and Ahmet S. Turk. 2016. “Avalanche Transistor Short Pulse Generator Trials for GPR.” Pp. 201–4 in *2016 8th International Conference on Ultrawideband and Ultrashort Impulse Signals (UWBUSIS)*.

Oppermann, Ian, Matti Hämäläinen, and Jari Iinatti. 2004. *UWB: Theory and Applications*. John Wiley \& Sons.

Pozar, David M. 2011. *Microwave Engineering*. John wiley \& sons.

Protiva, Pavel, Jan Mrkvica, and Jan Macháč. 2010. “A Compact Step Recovery Diode Subnanosecond Pulse Generator.” *Microwave and Optical Technology Letters* 52(2):438–40.

Razavi, Behzad, Turgut Aytur, Christopher Lam, Fei-Ran Yang, Kuang-Yu Li, Ran-Hong Yan, Han-Chang Kang, Cheng-Chung Hsu, and Chao-Cheng Lee. 2005. “A Uwb Cmos Transceiver.” *IEEE Journal of Solid-State Circuits* 40(12):2555–62.

Ross, G. 1968. “A Time Domain Criterion for the Design of Wideband Radiation Elements.” *IEEE Transactions on Antennas and Propagation* 16(3):355–56.

Ross, G. 1973. “Transmission and Reception System for Generating and Receiving

Base-Band Pulse Duration Pulse Signals without Distortion for Short Base-Band Communication System."

Ross, Gerald F. 1963. "The Transient Analysis of Multiple Beam Feed Networks for Array Systems." *Ph. D. Dissertation*.

Ross, Gerald F. 1966. "The Transient Analysis of Certain TEM Mode Four-Port Networks." *IEEE Transactions on Microwave Theory and Techniques* 14(11):528–42.

Sim, Sanghoon, Dong-Wook Kim, and Songcheol Hong. 2009. "A CMOS UWB Pulse Generator for 6--10 GHz Applications." *IEEE Microwave and Wireless Components Letters* 19(2):83–85.

Taylor, James D. 2012. *Ultrawideband Radar: Applications and Design*. CRC press.

Valizade, Arash, Pejman Rezaei, and Ali Asghar Orouji. 2017. "A Compact Reconfigurable Sub-Nanosecond Pulse Generator with Pulse-Shape Modulation." *International Journal of Microwave and Wireless Technologies* 9(4):741–45.

Vendelin, George D., Anthony M. Pavio, Ulrich L. Rohde, and Matthias Rudolph. 2021. *Microwave Circuit Design Using Linear and Nonlinear Techniques*. John Wiley \& Sons.

Wang, Li, Anxue Zhang, and Zhensheng Shi. 2020. "A High Voltage Pulse Generator Used in Ground Penetrating Radar." Pp. 1–3 in *2020 IEEE MTT-S International Wireless Symposium (IWS)*.

Wang, Qing, Xiaojian Tian, Yang Liu, Bo Li, and Bo Gao. 2008. "Design of an Ultra-Wideband Pulse Generator Based on Avalanche Transistor." Pp. 1–4 in *2008 4th International Conference on Wireless Communications, Networking and Mobile Computing*.

Wang, Qing, Xiaojian Tian, Jiangdong Shan, and Ge Wu. 2009. "Design of an Ultra-Short Pulse Generator." *Proceedings - 5th International Conference on Wireless Communications, Networking and Mobile Computing, WiCOM 2009* 17–19. doi: 10.1109/WICOM.2009.5305839.

Wong Choi, Gil, Jin Joo Choi, and Seung Hoon Han. 2011. "Note: Picosecond Impulse Generator Driven by Cascaded Step Recovery Diode Pulse Shaping Circuit." *Review of Scientific Instruments* 82(1):16106.

Wu, Qingping, and Wenchao Tian. 2010. "Design of Electronic Circuits of Nanosecond Impulser Based on Avalanche Transistor." *Proceedings - 2010 11th International Conference on Electronic Packaging Technology and High Density Packaging, ICEPT-HDP 2010* 774–77. doi: 10.1109/ICEPT.2010.5582702.

Xia, Xinfan, Lihua Liu, Hongfei Guan, and Guangyou Fang. 2013. "Balanced Pulse Generator for Ultra-Wideband Radar Application." *Electronics Letters* 49(4):293–95.

Yin, Qi, Zhongming Pan, and Zhuohang Zhang. 2018. "Design of a High-Performance Ultra-Wideband Monocycle Pulse Generator." in *2018 International Conference on Mechanical, Electronic, Control and Automation Engineering (MECAE 2018)*.

CURRICULUM VITAE

Personal Information

Name Surname : E**** T*****

Nationality : T.C.

Date and Place of Birth: …/…/1997 – M***** / T*****

Marital Status : S****

Phone : 0 506 … … 78

E-mail : em…….li@mu.edu.tr

: em…….li@yahoo.com

Education

Degree	Institution	Year
High-School	Muğla Gazi Anatolian High School	2011-2015
Bachelor	Karabük University – Dept. of Electrical and Electronics Engineering	2018-2020
Bachelor	Karabük University – Dept. of Biomedical Engineering	2015-2020
M.Sc.	Muğla Sıtkı Koçman University – Dept. of Electrical and Electronics Engineering	2021-Present

Work Experience

Year	Place	Enrollment
2018	Muğla Training and Research Hospital - Menteşe / Muğla	Trainee Biomedical Engineer
2019	ISBEM – Istituto Scientifico Biomedico Euro Mediterraneo Mesagne / İtalya	Trainee Biomedical Engineer
2020	Yatağan Termik Enerji A.Ş. Muğla / Türkiye	Trainee Electrical and Electronics Engineer
2021 – Present	Muğla Sıtkı Koçman University - Menteşe / Muğla	Research Assistant

Foreign Languages

English (Advanced)

Deutsch (Basic)

Computer and Programming Skills

ASP.NET, SQL, C#, Python, AutoCAD, KiCAD, OrCAD, SolidWorks, Microsoft Office.

Awards & Achievements

3rd top student in the Faculty of Engineering of Karabük University.

Top student in the department of Biomedical Engineering of Karabük University.

Publications

- Telli E., Şehirli E. 2020. "*Colon Automation System*" International Conference on Engineering Technologies (ICENTE'20).
- Telli Emrah, and Çam Taşkıran Zehra Gülru. 2022. "*A novel analysis and applications of an introduced hyperchaotic system*." Pamukkale Üniversitesi Mühendislik Bilimleri Dergisi 28.5 (2022): 701-709.